3.2.4 Typical results

Typical characteristic results are presented for the K11 concept and the bridge girder, pylon and the cable stays. The results are plotted for the load length dependent traffic loading (Q-Trf.sup), the upper bound traffic loading with max load intensity (Q-Trf-200m-inf.sup) and lower bound with min traffic load intensity (Q-Trf-1000m.sup).

For the bridge girder the weak axis bending moment is plotted, for the pylon the bending moment about transverse bridge axis for the west leg and spire is plotted, and normal forces in all stay cables.

Bridge girder

As one can see the weak axis moments for the bridge girder is close to the upper bound (load intensity based on L<=200m) for the span moments. This is due to the shorter influence lines of the uniformly distributed loads. The support moments at the pontoons have longer influence lines then 200m and one can account for a reduction here for these sections (see Figure 3-12). This is not the case for the abutment in north due to the one sided loading giving smaller influence lengths, see Figure 3-13.

Figure 3-10 Traffic loading, weak axis bending moment – comparison of envelope values for load length dependent traffic loading and infinite loaded length with 200m load intensity and 1000m load intensity.

Concept development, floating bridge E39 Bjørnafjorden
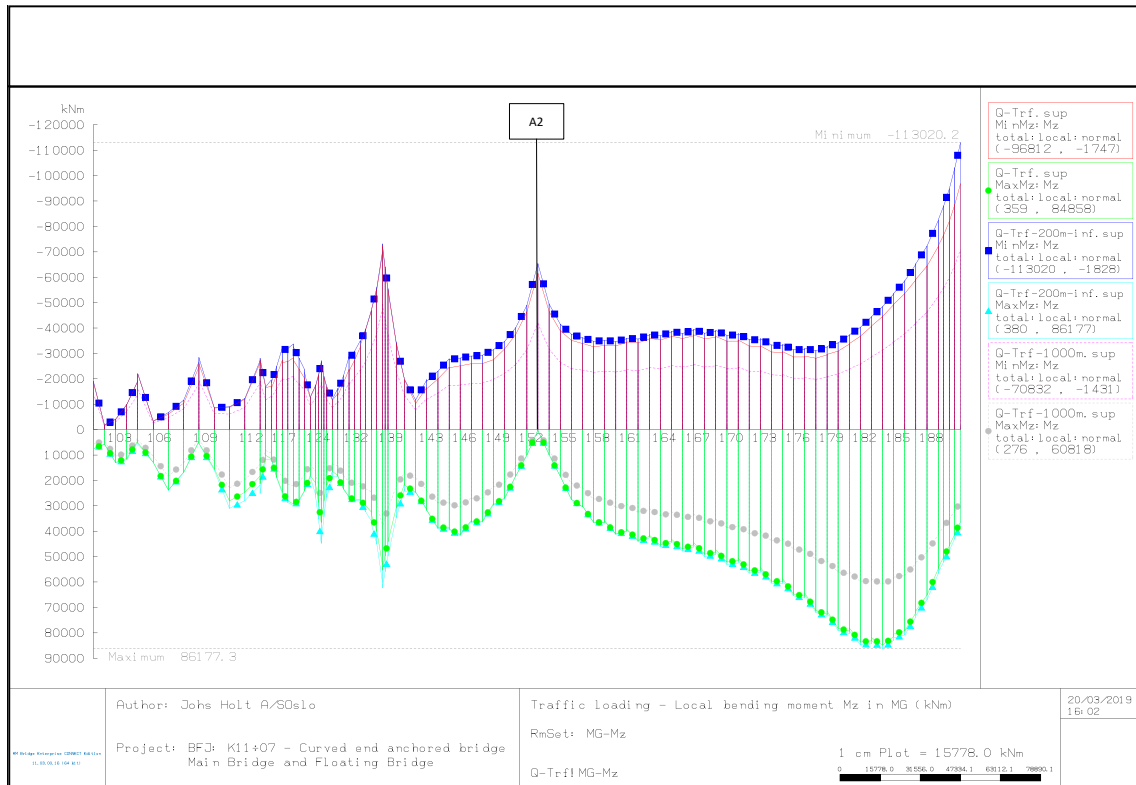
AMC status 2 – Variable static loads

Figure 3-11 Traffic loading, weak axis bending moment for the high-bridge – comparison of envelope values for load length dependent traffic loading and infinite loaded length with 200m load intensity and 1000m load intensity.
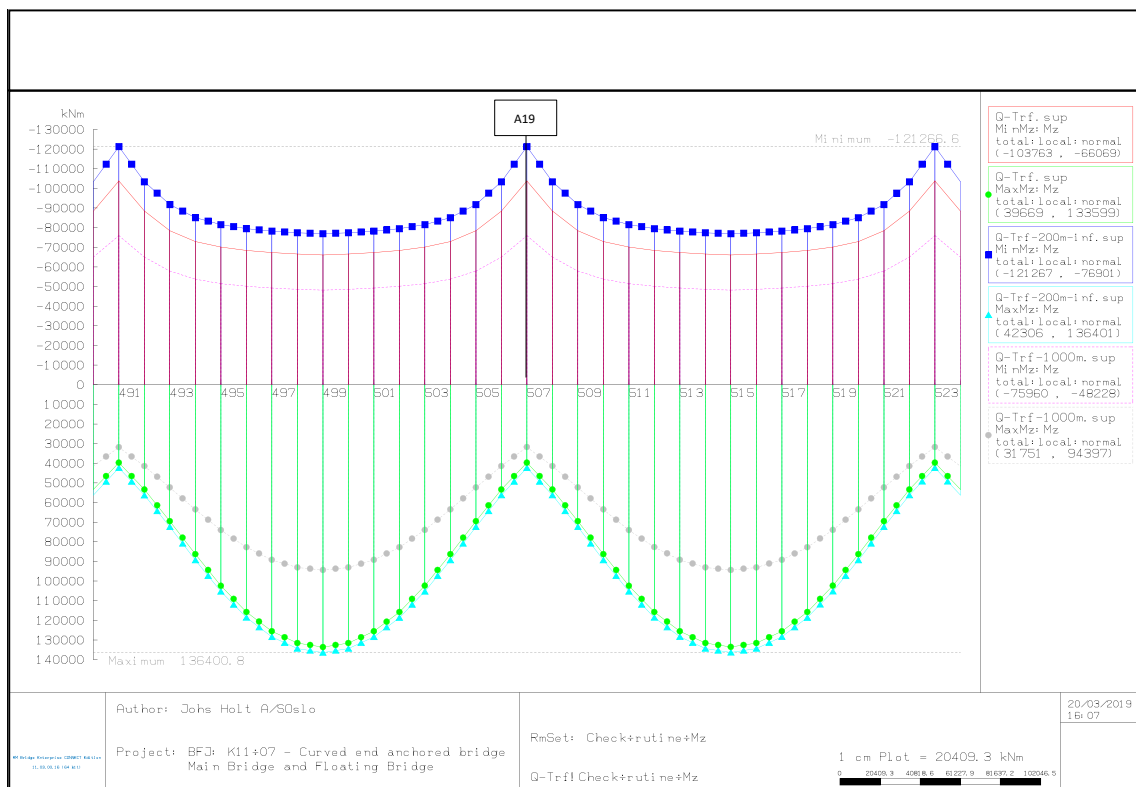

Figure 3-12 Traffic loading, weak axis bending moment typical floating span and supports – comparison of envelope values for load length dependent traffic loading and infinite loaded length with 200m load intensity and 1000m load intensity.
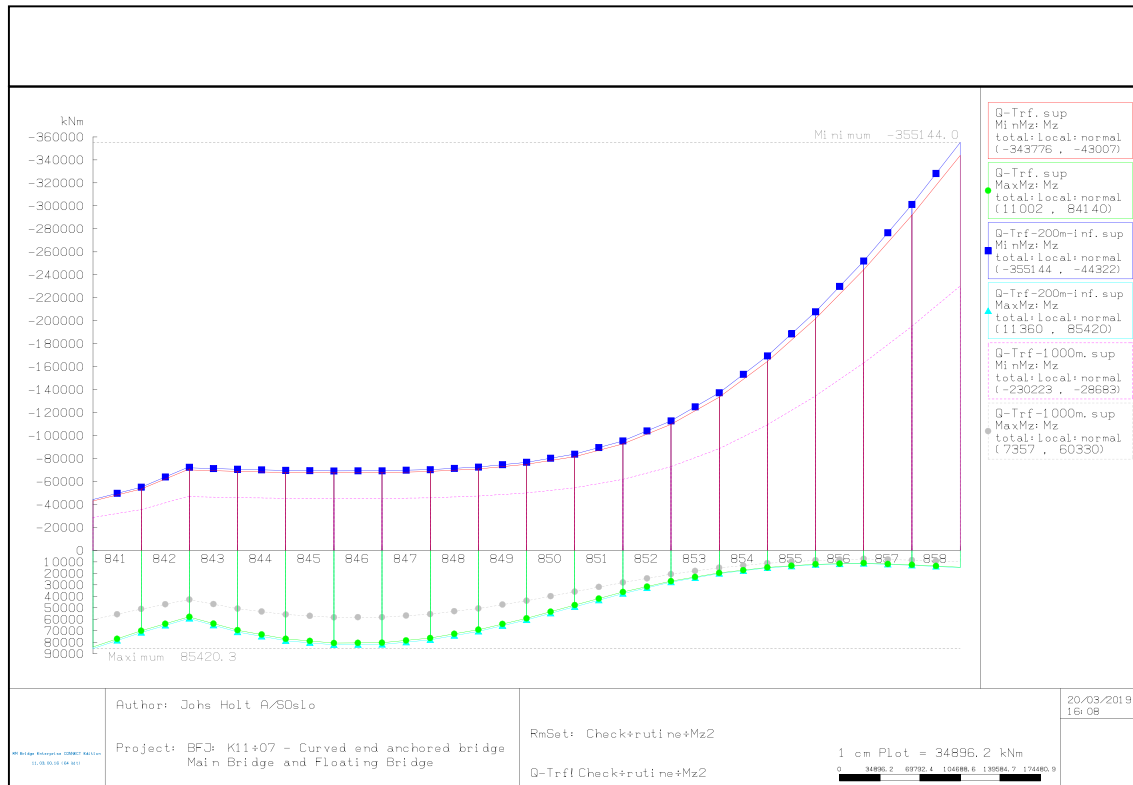
Figure 3-13 Traffic loading, weak axis bending moment abutment north– comparison of envelope values for load length dependent traffic loading and infinite loaded length with 200m load intensity and 1000m load intensity.

Pylon

Figure 3-14 Traffic loading, bending moment about transverse bridge axis in west pylon leg and spire – comparison of envelope values for load length dependent traffic loading and infinite loaded length with 200m load intensity and 1000m load intensity.
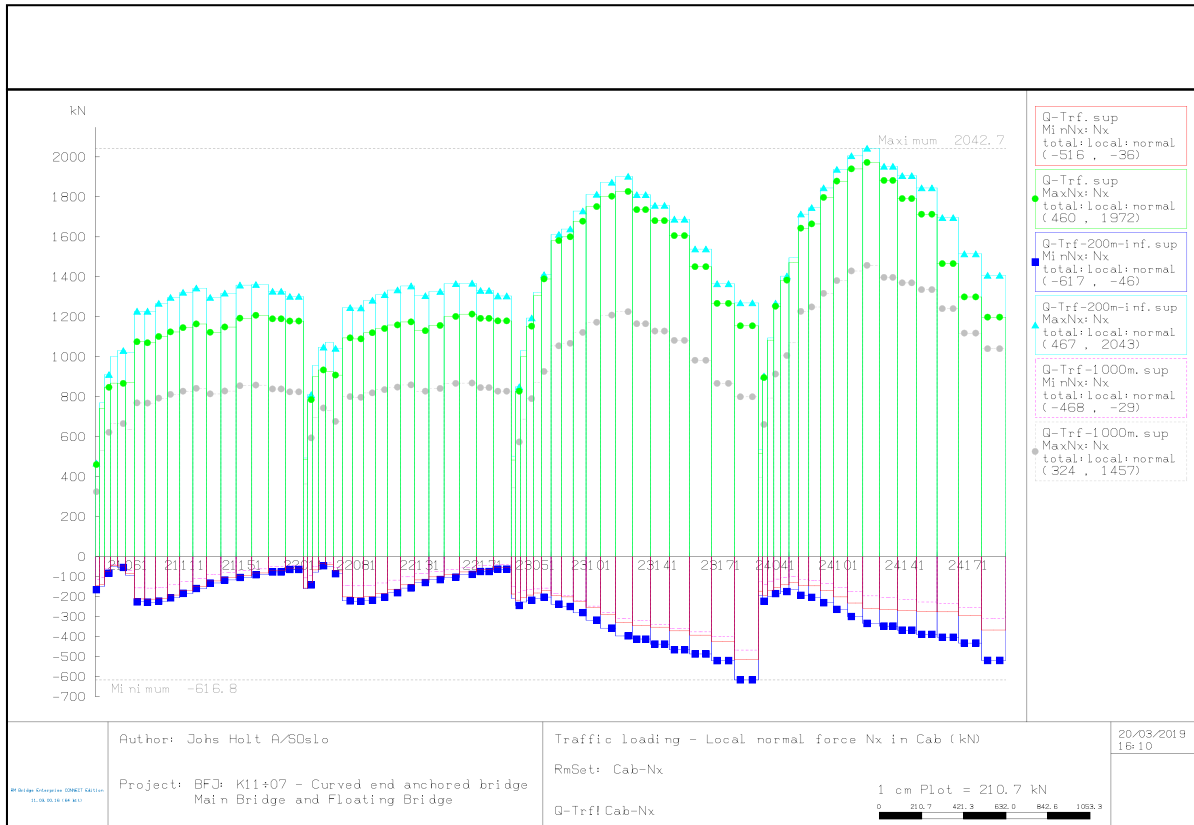
Stay cables

Figure 3-15 Traffic loading, normal forces in cable stays (21000- and 22000-seris are back span stays, 23000- and 24000-series are front span stays) – comparison of envelope values for load length dependent traffic loading and infinite loaded length with 200m load intensity and 1000m load intensity.

3.2.5 Roll end deformations in the bridge girder and pontoons

The criteria for max allowable roll due to traffic is 1 degree [Design Basis Bjørnafjorden, Table 10]. In Figure 3-16 the roll for the characteristic traffic loads (Q-Trf.sup) for the K11 concept is illustrated. The upper bound (Q-Trf-200m-inf.sup) and lower bound (Q-Trf-1000m.sup) are also included for illustration purpose. Since the traffic is plotted with characteristic values they should be multiplied with the combination factor 0.7. Hence, the maximum allowable roll for characteristic traffic is 1°/0.7=1.43° (=0.025rad). This criterion is met in the floating bridge north of axis 15, but not met south from axis 15 having a maximum rotation of 1.9° at axis 6. Note that the traffic are unfavourable placed on the bridge girder with the heaviest traffic on the shoulder. The design criterion is however for normal conditions. If one instead having the traffic placed centric in the traffic lanes according to Figure 2-1, the rotations due to traffic will decrease with an approximate factor of

$$\frac{\frac{13.5kN}{m} \cdot 8.5m + \frac{7.5kN}{m} \cdot 5.0m}{\frac{13.5kN}{m} \cdot 10.25m + \frac{7.5kN}{m} \cdot 7.25m} = \frac{\frac{152.25kNm}{m}}{\frac{192.75kNm}{m}} = 0.79$$

This will give a maximum rotation of the bridge girder of $1.9° \cdot 0.79 = 1.5°$, which is a small exceedance $\frac{1.5°}{1.43°} = 1.05$ locally around axis 6.
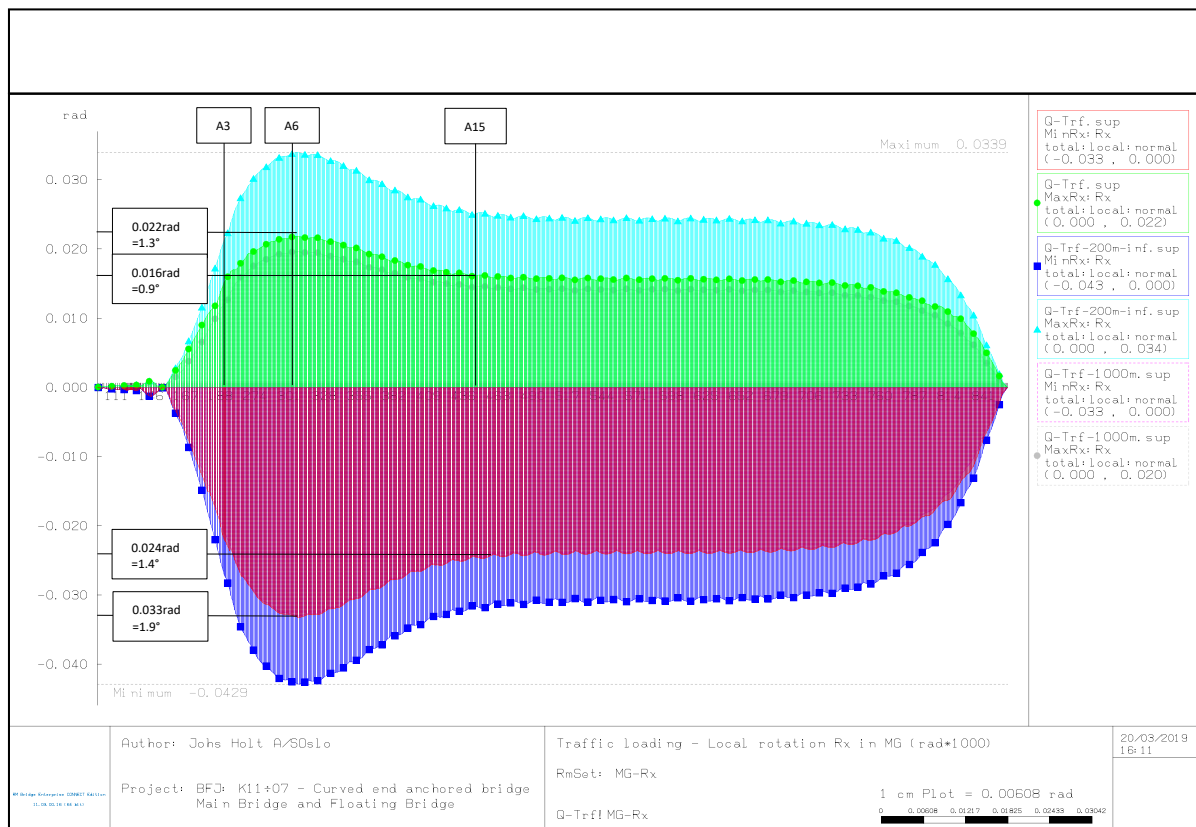

Figure 3-16 Traffic loading, rotation (roll) about the local bridge axis– comparison of envelope values for load length dependent traffic loading and infinite loaded length with 200m load intensity and 1000m load intensity.

The vertical deformation in the bridge girder from characteristic traffic loading is presented in Figure 3-17. The design criterion is that it should be less than 1.5m including combination factor 0.7 on the traffic. Hence, for characteristic traffic loading the criterion is $\frac{1.5m}{0.7} = 2.143m$. This criterion is met with an utilization rate $\frac{1.28m}{2.143m} = 0.6$.

Figure 3-17 Traffic loading, vertical deformation in bridge girder – comparison of envelope values for load length dependent traffic loading and infinite loaded length with 200m load intensity and 1000m load intensity.

Min/max roll and min/max vertical deformation and their associated roll and deformations is of interest when checking the freeboard of the pontoons. These results are plotted below in Figure 3-18 and Figure 3-19 for characteristic traffic loads.

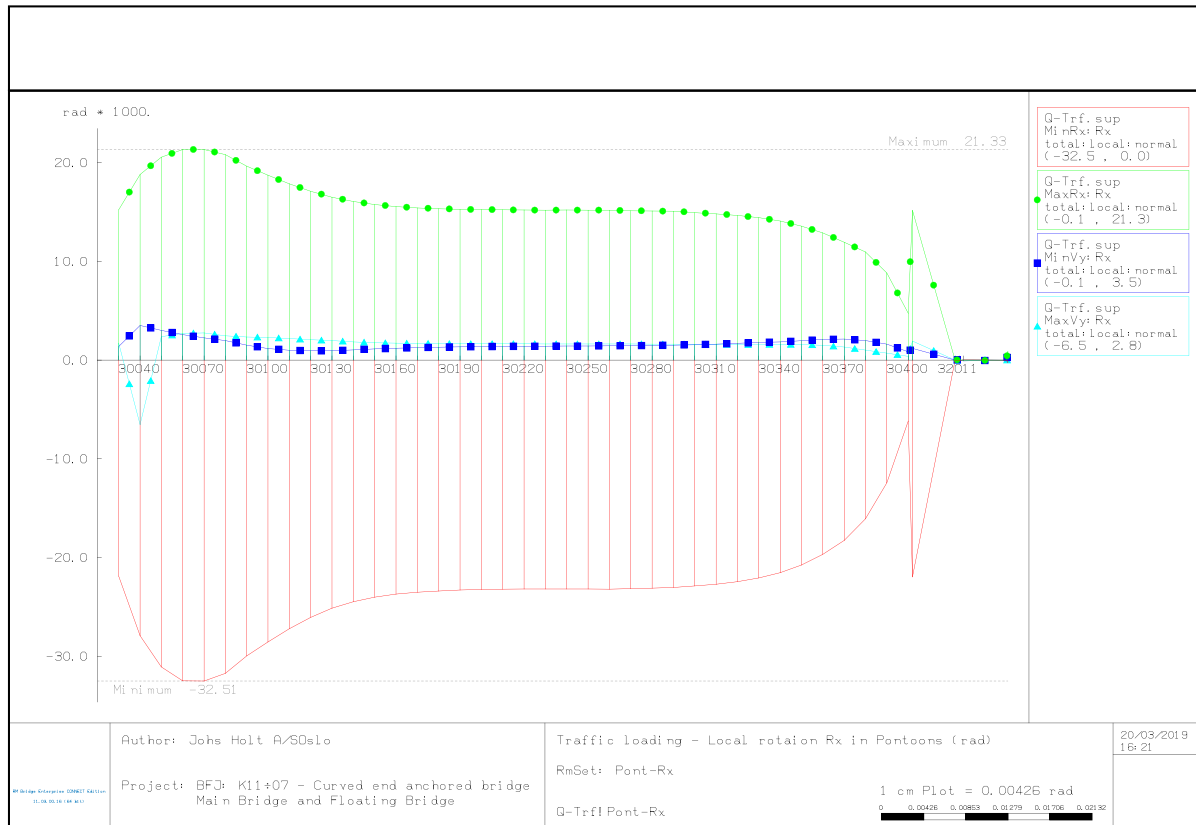*Figure 3-18 Traffic loading, rotation (roll) in pontoons about the local bridge axis– envelope values for load length dependent traffic sorted on Min/Max Roll and the Roll associated with Min/Max Vertical deformation*

Figure 3-19 Traffic loading, vertical deformation in pontoons – envelope values for load length dependent traffic sorted on Min/Max Vertical deformation and the Vertical deformation associated with Min/Max Roll

The largest roll angle is for the pontoon in axis 6. The largest edge displacement is of interest when checking the freeboard of the pontoon. The other pontoon give smaller values and are not presented here. For a pontoon width of $b = 58m$ the edge displacement is calculated as

$$Vy + \frac{b}{2} \cdot tan(Rx)$$

and presented below:

Table 3-16 Max vertical displacement at Pontoon 6

		Roll pontoon, Rx (rad)	Vert. disp. center pontoon, Vy (m)	Vert. displ. at pontoon edge (m)
Pontoon A6	MinRx	-0.033	-0.512	-1.455
	MaxRx	0.021	-0.540	-1.158
	MinVy	0.003	-1.123	-1.198
	MaxVy	0.003	0.070	0.148

3.2.6 Verification, hand calculations

The traffic results from RM-Bridge are confirmed by hand-calculations below. The chosen components is the weak axis span moments, the deflection and roll of the bridge girder in the floating part of the bridge. The answer differ between 0-3% which is satisfactory.

Bjørnafjorden - phase 5
Traffic loading
HT, 2019.03.15

Eurocode loads (LM1), loaded length $L < 200\ m$

$$q := 3\ \boldsymbol{m} \cdot (5.4 + 2.5 + 2.5 + 2.5 + 2.5 + 2.5 + 2.5)\ \frac{\boldsymbol{kN}}{\boldsymbol{m}^2} = 61.2\ \frac{\boldsymbol{kN}}{\boldsymbol{m}}$$

$$Q := 2 \cdot (300 + 200 + 100)\ \boldsymbol{kN} = 1200\ \boldsymbol{kN}$$

Pontoon stiffness (typical in the floating bridge part)

$$C_{33} := 7461.5\ \frac{\boldsymbol{kN}}{\boldsymbol{m}}$$

$$C_{44} := 1.113 \cdot 10^6\ \frac{\boldsymbol{kN} \cdot \boldsymbol{m}}{\boldsymbol{rad}}$$

Spanlength, girder

$$L := 125\ \boldsymbol{m}$$

$$I := \frac{\left(6 \cdot 4.317\ \boldsymbol{m}^4 + 10 \cdot 2.878\ \boldsymbol{m}^4\right)}{16} = 3.418\ \boldsymbol{m}^4 \qquad \text{(Average Second moment of inertia)}$$

$$E := 210\ \boldsymbol{GPa}$$

Load intensity pr. lane as function of loaded length $200\ m < L < 1000\ m$

$$q_1(qlen) := 5.4\ \frac{\boldsymbol{kN}}{\boldsymbol{m}^2} + \frac{(4.5 - 5.4)}{1000\ \boldsymbol{m} - 200\ \boldsymbol{m}}\ \frac{\boldsymbol{kN}}{\boldsymbol{m}^2} \cdot (qlen - 200\ \boldsymbol{m})$$

$$q_2(qlen) := 2.5\ \frac{\boldsymbol{kN}}{\boldsymbol{m}^2} + \frac{(2.5 - 2.5)}{1000\ \boldsymbol{m} - 200\ \boldsymbol{m}}\ \frac{\boldsymbol{kN}}{\boldsymbol{m}^2} \cdot (qlen - 200\ \boldsymbol{m})$$

$$q_3(qlen) := 2.5\ \frac{\boldsymbol{kN}}{\boldsymbol{m}^2} + \frac{(0 - 2.5)}{1000\ \boldsymbol{m} - 200\ \boldsymbol{m}}\ \frac{\boldsymbol{kN}}{\boldsymbol{m}^2} \cdot (qlen - 200\ \boldsymbol{m})$$

$$q_4(qlen) := 2.5\ \frac{\boldsymbol{kN}}{\boldsymbol{m}^2} + \frac{(2.5 - 2.5)}{1000\ \boldsymbol{m} - 200\ \boldsymbol{m}}\ \frac{\boldsymbol{kN}}{\boldsymbol{m}^2} \cdot (qlen - 200\ \boldsymbol{m})$$

$$q_5(qlen) := 2.5\ \frac{\boldsymbol{kN}}{\boldsymbol{m}^2} + \frac{(2.5 - 2.5)}{1000\ \boldsymbol{m} - 200\ \boldsymbol{m}}\ \frac{\boldsymbol{kN}}{\boldsymbol{m}^2} \cdot (qlen - 200\ \boldsymbol{m})$$

$$q_6(qlen) := 2.5\ \frac{\boldsymbol{kN}}{\boldsymbol{m}^2} + \frac{(0 - 2.5)}{1000\ \boldsymbol{m} - 200\ \boldsymbol{m}}\ \frac{\boldsymbol{kN}}{\boldsymbol{m}^2} \cdot (qlen - 200\ \boldsymbol{m})$$

$$q_f(qlen) := 2.5\ \frac{\boldsymbol{kN}}{\boldsymbol{m}^2} + \frac{(0.625 - 2.5)}{1000\ \boldsymbol{m} - 200\ \boldsymbol{m}}\ \frac{\boldsymbol{kN}}{\boldsymbol{m}^2} \cdot (qlen - 200\ \boldsymbol{m})$$

$$q(qlen) := 3\ \boldsymbol{m}\ \left(q_1(qlen) + q_2(qlen) + q_3(qlen) + q_4(qlen) + q_5(qlen) + q_6(qlen) + q_f(qlen)\right)$$

Plot, load intensity as function of loaded length

$qlen := 200 \ \boldsymbol{m}, 201 \ \boldsymbol{m} .. 1000 \ \boldsymbol{m}$

$q(qlen) \left(\dfrac{\boldsymbol{kN}}{\boldsymbol{m}} \right)$

$qlen \ (\boldsymbol{m})$
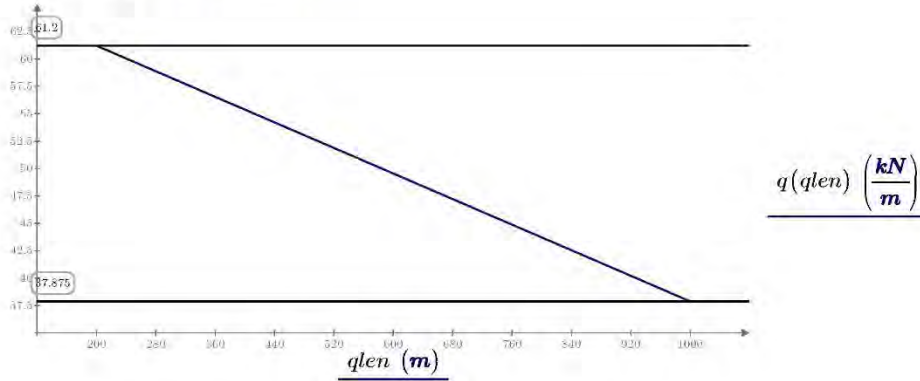
Beam on elastic bed (three equal spans) - [Handboken Bygg - Byggtabeller]

Span moment

$qlen := 200 \ \boldsymbol{m}$ $\qquad$ $q(qlen) = 61.2 \ \dfrac{\boldsymbol{kN}}{\boldsymbol{m}}$ $\qquad$ (Loaded length and load intensity)

$\mu := \dfrac{48 \cdot E \cdot I}{L^3 \cdot C_{33}} = 2.364$

$f_A := -0.0357 + \dfrac{(-0.0109 - -0.0357)}{(3-1)} \cdot (\mu - 1) = -0.019$ $\qquad$ (Assume linear variation between $\mu = 1$ and $\mu = 3$)

$f_B := 0.5357 + \dfrac{(0.5109 - 0.5357)}{(3-1)} \cdot (\mu - 1) = 0.519$

$R_{A.q} := f_A \cdot q(qlen) \cdot L = -143.726 \ \boldsymbol{kN}$

$R_{B.q} := f_B \cdot q(qlen) \cdot L = 3.969 \ \boldsymbol{MN}$

$R_{A.Q} := f_A \cdot Q = -22.545 \ \boldsymbol{kN}$

$R_{B.Q} := f_B \cdot Q = 0.623 \ \boldsymbol{MN}$

$M_{span.q} := \dfrac{-q(qlen) \cdot L^2}{8} + \dfrac{R_{B.q} \cdot L}{2} + \dfrac{R_{A.q} \cdot 3 \ L}{2} = 101.566 \ \boldsymbol{MN \cdot m}$ $\qquad$ $\dfrac{q(qlen) \cdot L^2}{M_{span.q}} = 9.415$

$M_{span.Q} := \dfrac{R_{B.Q} \cdot L}{2} + \dfrac{R_{A.Q} \cdot 3 \ L}{2} = 34.682 \ \boldsymbol{MN \cdot m}$ $\qquad$ $\dfrac{Q \cdot L}{M_{span.Q}} = 4.325$

$$M_{span} := M_{span.q} + M_{span.Q} = 136.247 \ MN \cdot m$$

$$\left(\frac{133.599 \ MN \cdot m}{M_{span}} \right) = 0.981$$

(Compared to RM-Bridge analyses, see Figure 3-12)

Bridge girder deflection

$$qlen := 380 \ m \qquad\qquad q(qlen) = 55.952 \ \frac{kN}{m}$$

(Loaded length and load intensity)

$$\delta_{sup} := \frac{q(qlen) \cdot L + Q}{C_{33}} = 1098.169 \ mm$$

$$\left(\frac{1124 \ mm}{\delta_{sup}} \right) = 1.024$$

(Compared to RM-Bridge analyses, see Figure 3-17)

$$\delta_{span} := q(qlen) \cdot \left(\frac{L}{C_{33}} + \frac{5 \ L^4}{384 \cdot E \cdot I} \right) + Q \ \frac{L^3}{48 \cdot E \cdot I} = 1253.205 \ mm$$

$$\left(\frac{1275 \ mm}{\delta_{span}} \right) = 1.017$$

(Compared to RM-Bridge analyses, see Figure 3-17)

Bridge girder rotations

$$qlen := 1000 \ m \qquad\qquad q(qlen) = 37.875 \ \frac{kN}{m}$$

(Loaded length and load intensity)

$$M_t := 3 \ m \cdot L \cdot \left(q_1(qlen) \cdot (10.25 \ m) + q_2(qlen) \cdot 7.25 \ m + q_3(qlen) \cdot 4.25 \ m \right) \lrcorner = 26568.75 \ kN \cdot m$$
$$+ \frac{(600 \ kN \cdot 10.25 \ m + 400 \ kN \cdot 7.25 \ m + 200 \ kN \cdot 4.25 \ m)}{4}$$

$$\theta := \frac{M_t}{C_{44}} = 0.024 \ rad \qquad \theta = 1.368 \ deg \qquad\qquad 0.7 \ \theta = 0.957 \ deg$$

$$\left(\frac{0.024 \ rad}{\theta} \right) = 1.005$$

(Compared to RM-Bridge analyses, see Figure 3-16)

3.3   Temperature analysis in RM Bridge

3.3.1   Temperature load combinations

Combination rules

SupAddLc - Unconditional adding of the results of the specified load case to the contents of the treated superposition file.

SupAndLc - Conditional adding of the Load Case result values to the contents of the treated superposition file (if they are unfavorable)

SupAndSup - Conditional adding of the result values of an envelope to the contents of the treated superposition file (if they are unfavorable).

SupOrLc - Conditional replacement of the current envelope result values by the Load Case result values (if they are more unfavorable).

SupOrSup - Conditional replacement of the current envelope result values by the result values of the envelope being superimposed (if they are more unfavorable).

Temperature loading cases

Temperature loading cases (index s=steel, c=concrete sections):

Table 3-17 Single temperature load cases

LoadCase	Description
q-temp-max	Temperature - max temperature (Ts=39, Tc=20)
q-temp-min	Temperature - min temperature (Ts=-30, Tc=-19)
q-temp-topgrad	Temperature - gradient, varmer toppside (Tgs=12.6, Tgc=7)
q-temp-botgrad	Temperature - gradient, varmer bottomside (Tgs=-15.6, Tgc=-5)
q-temp-fut	Temperature - future increase on Tmax (T=2)
q-temp-cables	Temperature - structure temperature difference (T=10)

The temperature gradient in the concrete beam and the stay cable bridge is based on cross-section height of 3.5m and the floating bridge on cross-section height 4m.

To account for the max temperature and a possible future increase in temperature a sup-file as follows:

Table 3-18 Max temperature and future increase in air temperature

Sup-file	Combination rule	Sup-file
Q-Temp-Max.sup	SupAddLc	q-temp-max
	SupAndLc	q-temp-fut

The temperature difference between the stay cables and the other construction parts are stored in sup-file as follows:

Table 3-19 Temperature difference between stay cables and the rest of the construction

Sup-file	Combination rule	Sup-file
q-temp-cables.sup	SupOrLc	1.0*(q-temp-cables)
	SupOrLc	-1.0*(q-temp-cables)

Temperature load combinations

Table 3-20 Temperature load combinations

Sup-file	Combination rule	Sup-file
q-temp-comb1.sup	SupAndSup	Q-Temp-Max.sup
	SupOrLc	q-temp-min
	SupOrLc	q-temp-topgrad
	SupOrLc	q-temp-botgrad
q-temp-comb2.sup	SupAndLc	q-temp-topgrad
	SupAndSup	0.35*(Q-Temp-Max.sup)
q-temp-comb3.sup	SupAndLc	q-temp-topgrad
	SupAndLc	0.35*(q-temp-min)
q-temp-comb4.sup	SupAndLc	q-temp-botgrad
	SupAndSup	0.35*(Q-Temp-Max.sup)
q-temp-comb5.sup	SupAndLc	q-temp-botgrad
	SupAndLc	0.35*(q-temp-min)
q-temp-comb6.sup	SupAndSup	Q-Temp-Max.sup
	SupAndLc	0.75*(q-temp-topgrad)
q-temp-comb7.sup	SupAndSup	Q-Temp-Max.sup
	SupAndLc	0.75*(q-temp-botgrad)
q-temp-comb8.sup	SupAndLc	q-temp-min
	SupAndLc	0.75*(q-temp-topgrad)
q-temp-comb9.sup	SupAndLc	q-temp-min
	SupAndLc	0.75*(q-temp-botgrad)

To have the max and minimum response the must unfavourable of the combinations above the worst combination above is chosen and finally the temperature difference of stay cables is added if unfavourable.

Table 3-21 Temperature load combination

Sup-file	Combination rule	Sup-file

Q-Temp.sup	SupAndSup	q-temp-comb1.sup
	SupOrSup	q-temp-comb2.sup
	SupOrSup	q-temp-comb3.sup
	SupOrSup	q-temp-comb4.sup
	SupOrSup	q-temp-comb5.sup
	SupOrSup	q-temp-comb6.sup
	SupOrSup	q-temp-comb7.sup
	SupOrSup	q-temp-comb8.sup
	SupOrSup	q-temp-comb9.sup
	SupAndSup	q-temp-cables.sup

3.3.2 Typical results

Typical characteristic temperature results are presented below for the four different concepts K11, K12, K13 and K14. The results are given for the bridge girder in their local coordinate systems.

The results presented are the transverse displacements, normal force and weak and strong axis bending moments.
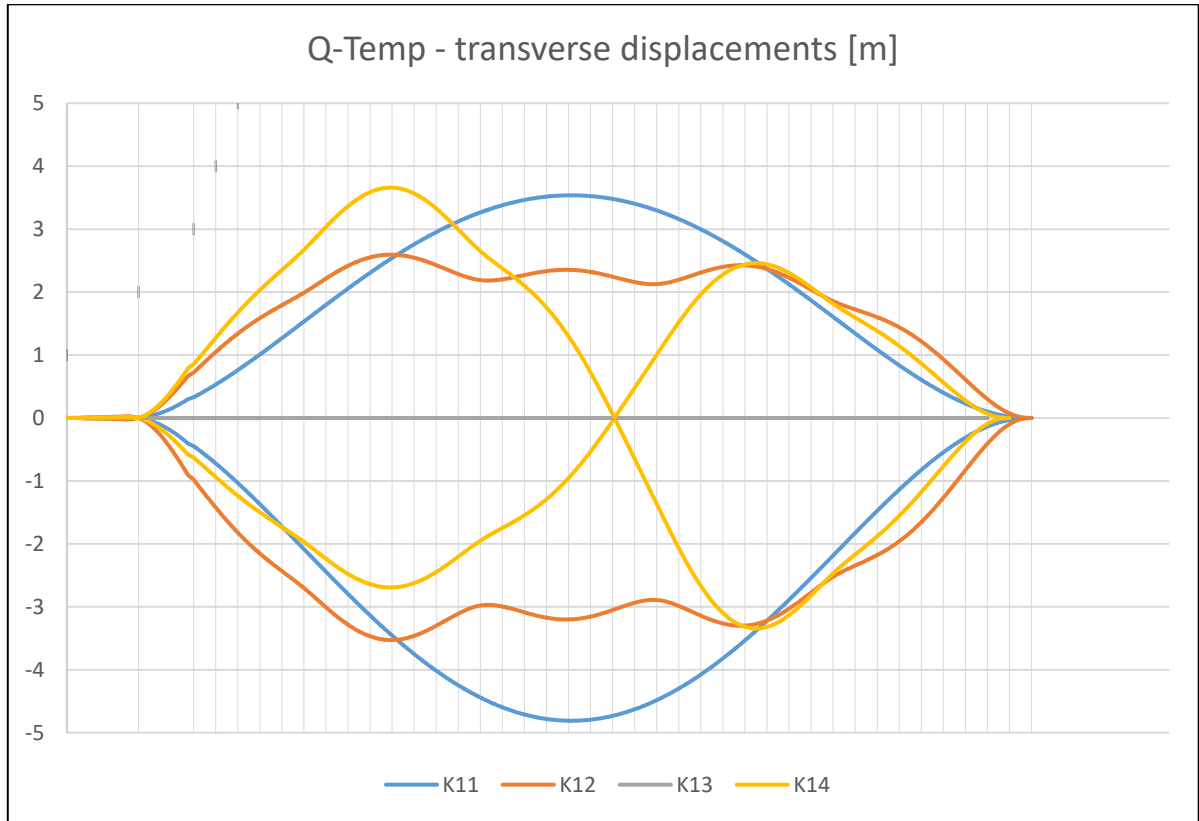

Figure 3-20 Temperature loading – transverse displacement in bridge girder [m]
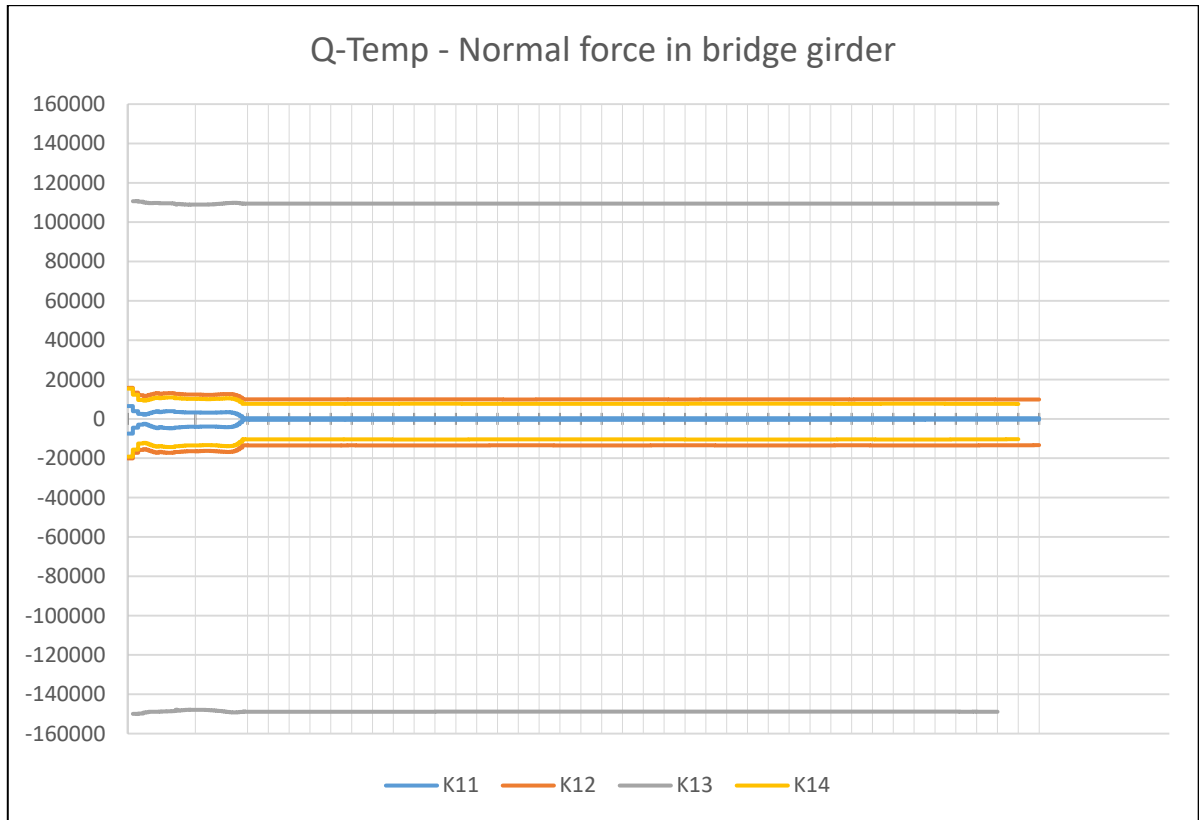
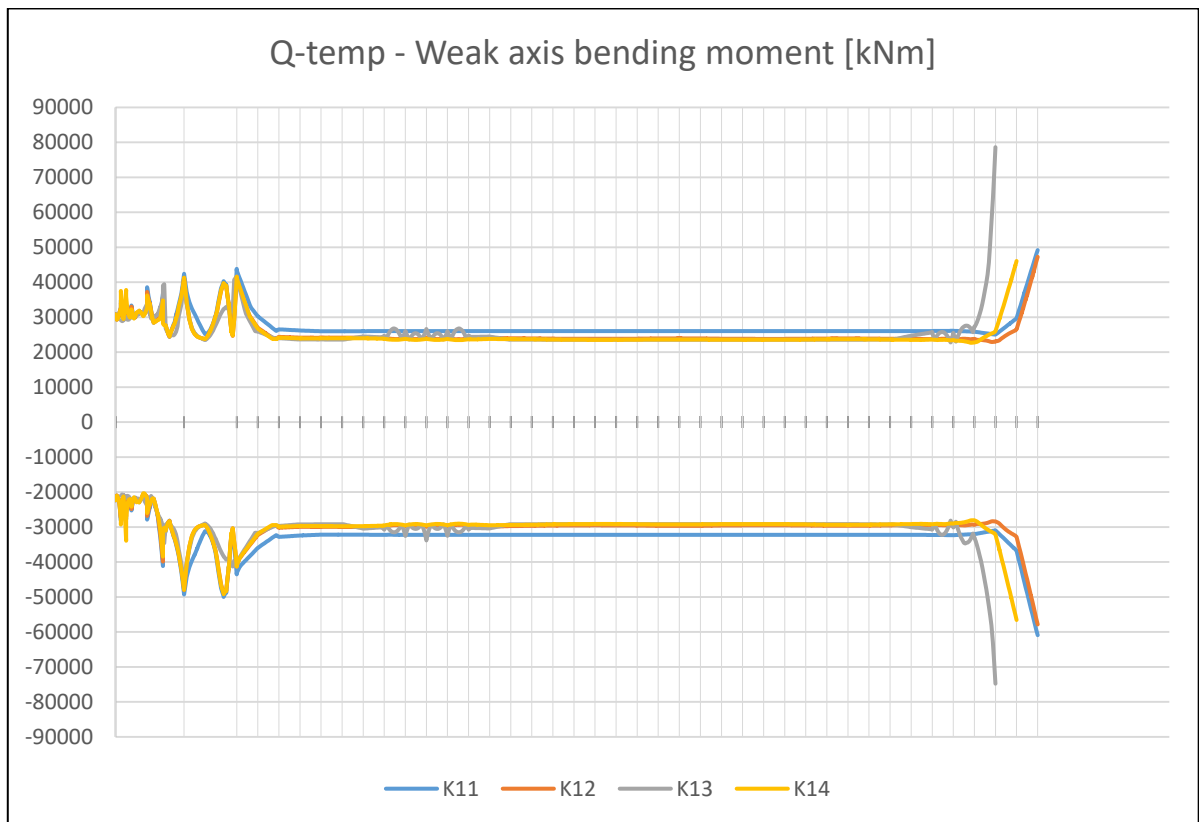*Figure 3-21 Temperature loading – normal force in bridge girder [kN]*

Figure 3-22 Temperature loading – weak axis bending in bridge girder [kNm]
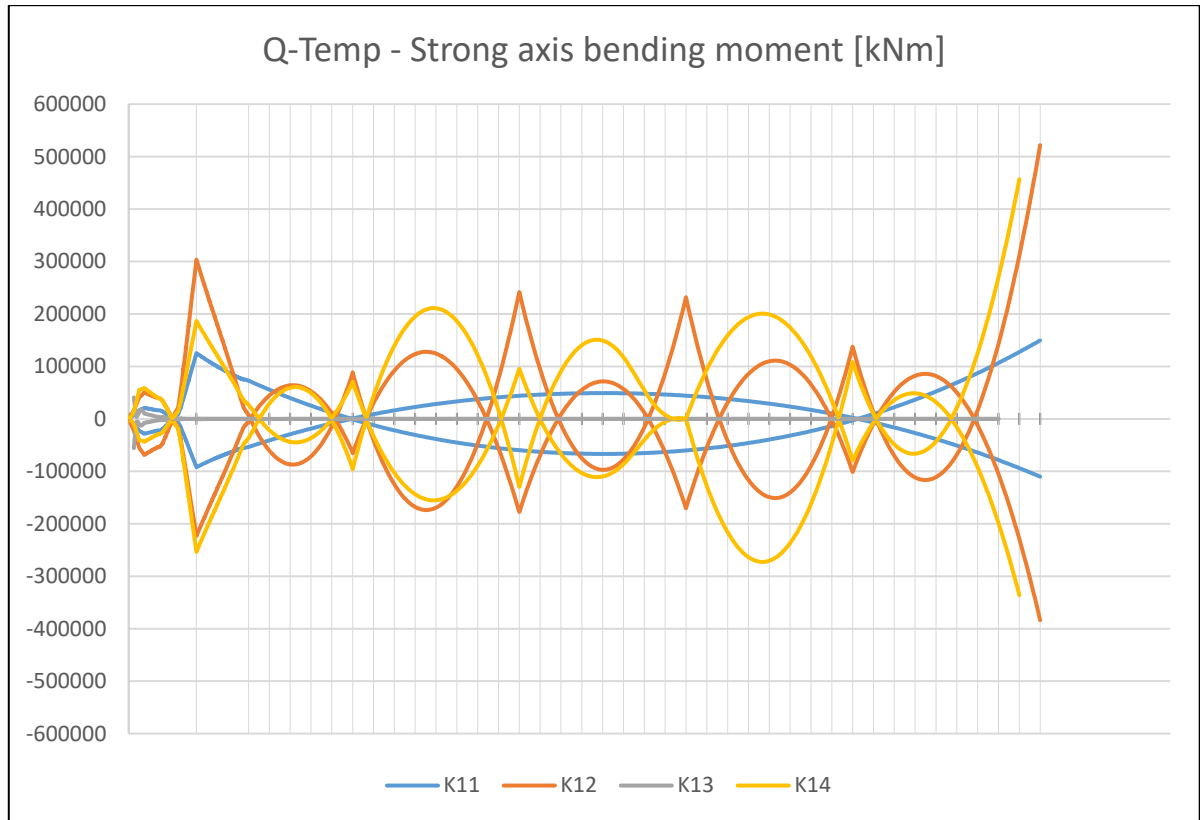
Figure 3-23 Temperature loading – strong axis bending in bridge girder [kNm]

3.3.3 Verification, hand calculations

Bjørnafjorden - phase 5
Temperature loading
HT, 2019.03.15

Thermal loads (Designbasis MetOcean, rev1)

$$T_{max} := 33$$

$$T_{min} := -17$$

Design thermal loads (Steel cross-section - Type 1)

$$T_0 := 10$$

$$T_{e.max} := T_{max} + 16 = 49 \qquad \text{[NS-EN 1991-1-5, Figure NA.6.1]}$$

$$T_{e.min} := T_{min} - 3 = -20 \qquad \text{[NS-EN 1991-1-5, Figure NA.6.1]}$$

$$\Delta T_{N.con} := -(T_0 - T_{e.min}) = -30 \qquad \text{[NS-EN-1-5, eq. (6.1)]}$$

$$\Delta T_{N.exp} := T_{e.max} - T_0 = 39 \qquad \text{[NS-EN-1-5, eq. (6.2)]}$$

$$\Delta T_{M.heat} := 0.7 \cdot 18 = 12.6 \qquad \text{[NS-EN 1991-1-5, table NA.6.1 adn NA.6.2]}$$

$$\Delta T_{M.cool} := -(1.2 \cdot 13) = -15.6 \qquad \text{[NS-EN 1991-1-5, table NA.6.1 adn NA.6.2]}$$

Spanlength and bridge girder properties

$$L := 4913.532 \; \boldsymbol{m} \qquad\qquad \text{Chord length (between pylon and north abutment)}$$

$$R := 5000 \; \boldsymbol{m} \qquad\qquad \text{Radius}$$

$$f := R - \sqrt{R^2 - \left(\frac{L}{2}\right)^2} = 645.198 \; \boldsymbol{m} \qquad\qquad \text{Sagitta heigth}$$

$$\theta := \operatorname{asin}\left(\frac{\left(\frac{L}{2}\right)}{R}\right) = 29.43 \; \boldsymbol{deg} \qquad\qquad \text{Angle between chord and arch}$$

$$h := 4 \; \boldsymbol{m} \qquad\qquad \text{Bridge girder, cross-section height}$$

$$A := \frac{6 \cdot 2.0974 \; \boldsymbol{m}^2 + 10 \cdot 1.4271 \; \boldsymbol{m}^2}{16} = 1.678 \; \boldsymbol{m}^2 \qquad\qquad \text{Average cross-section area, bridge girder}$$

$$I_y := \frac{\left(6 \cdot 135.49 \; \boldsymbol{m}^4 + 10 \cdot 107.23 \; \boldsymbol{m}^4\right)}{16} = 117.828 \; \boldsymbol{m}^4 \qquad\qquad \text{Average second moment of inertia, bridge girder - strong axis}$$

$$I_z := \frac{\left(6 \cdot 4.317 \; \boldsymbol{m}^4 + 10 \cdot 2.878 \; \boldsymbol{m}^4\right)}{16} = 3.418 \; \boldsymbol{m}^4 \qquad\qquad \text{Average Second moment of inertia, bridge girder - weak axis}$$
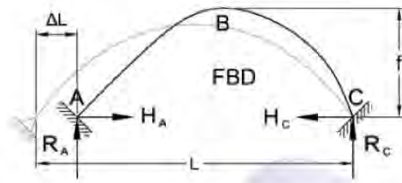
Material properties

$$E := 210 \ \textbf{GPa}$$

$$\alpha := 1.2 \cdot 10^{-5}$$

Load effect - Max uniform temperature expansion $\Delta T_{N.exp} = 39$

ΔL	"Support movement" due to temperature
H_A	Horizontal reaction force at support
$M_{y.A}$	Support moment at support A (equal C)
$M_{y.B}$	Span moment at section B

$$\Delta L := \alpha \cdot \Delta T_{N.exp} \cdot L = 2.3 \ \textbf{m}$$

$$H_A := \frac{45}{4} \left(\frac{E \cdot I_y}{f^2 \cdot L} \right) \cdot \Delta L = 312.952 \ \textbf{kN}$$

$$M_{y.A} := \frac{15}{2 \ f} \cdot \left(\frac{E \cdot I_y}{L} \right) \cdot \Delta L = 134.611 \ \textbf{MN} \cdot \textbf{m}$$

$$\left(\frac{141.836 \ \textbf{MN} \cdot \textbf{m}}{M_{y.A}} \right) = 1.054$$ (Compared to RM-Bridge analyses)

$$M_{y.B} := M_{y.A} - H_A \cdot f = -67.305 \ \textbf{MN} \cdot \textbf{m}$$

$$\left(\frac{-63.284 \ \textbf{MN} \cdot \textbf{m}}{M_{y.B}} \right) = 0.94$$ (Compared to RM-Bridge analyses)

$$w_B := \frac{2 \cdot \Delta L \cdot L}{\pi^2 \cdot f} = 3.549 \ \textbf{m}$$

$$\left(\frac{4.56 \ \textbf{m}}{w_B} \right) = 1.285$$ (Compared to RM-Bridge analyses. The larger deviation here is probably due to that the bridge-girder is not fully fixed to the pylon as assumed in hand calculations. Therefore, larger displacments is expected in the analysis)

Load effect - Max uniform temperature expansion $\Delta T_{N.con} = -30$

$$\Delta L := \alpha \cdot \Delta T_{N.con} \cdot L = -1.769 \; \boldsymbol{m}$$

$$H_A := \frac{45}{4} \left(\frac{E \cdot I_y}{f^2 \cdot L} \right) \cdot \Delta L = -240.733 \; \boldsymbol{kN}$$

$$M_{y.A} := \frac{15}{2 \, f} \cdot \left(\frac{E \cdot I_y}{L} \right) \cdot \Delta L = -103.547 \; \boldsymbol{MN \cdot m}$$

$$\left(\frac{-109.726 \; \boldsymbol{MN \cdot m}}{M_{y.A}} \right) = 1.06 \qquad \text{(Compared to RM-Bridge analyses)}$$

$$M_{y.B} := M_{y.A} - H_A \cdot f = 51.773 \; \boldsymbol{MN \cdot m}$$

$$\left(\frac{48.947 \; \boldsymbol{MN \cdot m}}{M_{y.B}} \right) = 0.945 \qquad \text{(Compared to RM-Bridge analyses)}$$

$$w_B := \frac{2 \cdot \Delta L \cdot L}{\pi^2 \cdot f} = -2.73 \; \boldsymbol{m}$$

$$\left(\frac{-3.53 \; \boldsymbol{m}}{w_B} \right) = 1.293 \qquad \text{(Compared to RM-Bridge analyses. The larger deviation here is probably due to that the bridge-girder is not fully fixed to the pylon as assumed in hand calculations. Therefore, larger displacments is expected in the analysis)}$$

Temperature gradient - warmer top side $\Delta T_{M.heat} = 12.6$

$$\kappa := \frac{\Delta T_{M.heat} \cdot \alpha}{h} = \left(3.78 \cdot 10^{-5} \right) \frac{1}{\boldsymbol{m}}$$

$$M_z := \kappa \cdot E \cdot I_z = 27.129 \; \boldsymbol{MN \cdot m}$$

$$\left(\frac{26.025 \; \boldsymbol{MN \cdot m}}{M_z} \right) = 0.959 \qquad \text{(Compared to RM-Bridge analyses)}$$

Temperature gradient - warmer bottom side $\Delta T_{M.cool} = -15.6$

$$\kappa := \frac{\Delta T_{M.cool} \cdot \alpha}{h} = -4.68 \cdot 10^{-5} \frac{1}{\boldsymbol{m}}$$

$$M_z := \kappa \cdot E \cdot I_z = -33.588 \; \boldsymbol{MN \cdot m}$$

$$\left(\frac{-32.221 \; \boldsymbol{MN \cdot m}}{M_z} \right) = 0.959 \qquad \text{(Compared to RM-Bridge analyses)}$$

Concept development, floating bridge

E39 Bjørnafjorden

Appendix G – Enclosure 15

10205546-11-NOT-193

Long-term wave response

MEMO

PROJECT	Concept development, floating bridge E39 Bjørnafjorden	DOCUMENT CODE	10205546-11-NOT-193
CLIENT	Statens vegvesen	ACCESSIBILITY	Restricted
SUBJECT	Long-term wave response	PROJECT MANAGER	Svein Erik Jakobsen
TO	Statens vegvesen	PREPARED BY	Finn-Idar Grøtta Giske Bernt Sørby
COPY TO		RESPONSIBLE UNIT	AMC

SUMMARY

In this document the estimation of response values with a specified return period is discussed. The underlying theory is presented, and the relation between different solution methods is explained. Finally, some results are presented for the concept K12_07 in order to assess the validity of the contour line approach. The results indicate that the extreme response estimates produced by the contour method might be too rough. However, it is not possible to draw any definite conclusion without a comparison with the full long-term approach.

0	15.08.2019	Final issue	F. I. G. Giske, B. Sørby	M. Storheim	S. E. Jakobsen
REV.	DATE	DESCRIPTION	PREPARED BY	CHECKED BY	APPROVED BY

Table of Contents

1 Long-term wave response

The ultimate goal of a long-term response analysis is to identify the response value with a given return period. More specifically, we seek the characteristic response value r_q, which has a specified annual exceedance probability q. This is referred to as the q-probability response or the $1/q$-year response. For instance, the 100-year response has a probability $q = 0.01$ of being exceeded during any year, which means that it is exceeded in average once every 100 years.

The q-probability response is most accurately determined by a full long-term approach [1]. However, due to the large computational cost associated with this approach, the environmental contour method, sometimes referred to as the short-term design approach, is commonly used to obtain reasonable estimates of the q-probability response. Recently, methods have been developed which provide more accurate estimates of the q-probability response at a significantly reduced computational cost [2, 3]. These methods are referred to as inverse reliability methods. In this section, the relation between the full long-term approach, the environmental contour method and the inverse reliability methods is explained.

1.1 Full long-term approach

The long-term situation is considered a collection of $\widetilde{N}$ short-term states, each of duration $\widetilde{T} = 1$ hr, as illustrated in Figure 1-1. For a duration of one year we then have $\widetilde{N} = 365.25 \cdot 24 = 8766$ short-term states. Assuming independence between the short-term states, the q-probability response r_q is found by requiring

$$\Pr\left[\text{Largest response during one year} > r_q\right] = 1 - \Pr\left[\tilde{R} \leq r_q\right]^{\widetilde{N}} = 1 - F_{\tilde{R}}(r)^{\widetilde{N}} = q, \tag{1}$$

where $F_{\tilde{R}}(r)$ is the distribution of the largest response $\tilde{R}$ in a randomly chosen short-term state. This distribution can be referred to as the long-term distribution of the short-term maximum response or simply the average short-term distribution. The requirement in Eqn. (1) can be rewritten as $F_{\tilde{R}}(r_q) = (1 - q)^{1/\widetilde{N}} \approx 1 - q/\widetilde{N}$, which is practically an equality when q is small and $\widetilde{N}$ is large.

The long-term distribution $F_{\tilde{R}}(r)$ of the 1-hour maximum response must take into account two sources of randomness: The randomness due to different probability of occurrence for different sea states (the environmental model), and the randomness due to variability in the 1-hour max for different realizations of the same sea state (short-term extreme value distribution).
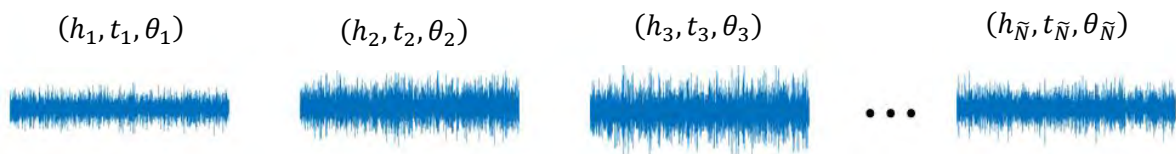
$$(h_1, t_1, \theta_1) \qquad (h_2, t_2, \theta_2) \qquad (h_3, t_3, \theta_3) \qquad (h_{\widetilde{N}}, t_{\widetilde{N}}, \theta_{\widetilde{N}})$$

Figure 1-1 The long-term situation is modelled as a collection of $\widetilde{N}$ independent short-term states with constant sea state parameters (h, t, θ) within each state.

1.1.1 Environmental model

A short-term state is specified by the sea state parameters $\left(H_s, T_p, \overline{\Theta}\right)$, i.e. significant wave height, peak period and mean wave direction respectively, and these are assumed constant within each short-term state. The probability of occurrence for different sea states is determined by data from the location. The occurrence probabilities are given in scatter diagrams in the metocean design basis [4], as illustrated in Figure 1-2, but a joint probability density function (PDF) $f_{H_s, T_p, \overline{\Theta}}(h, t, \theta)$ can also be fitted to the data. Such a fitting of an environmental model will usually be necessary for

a long-term analysis since the amount of data is limited to a few years and we are interested in events with return periods of 100 or even 10 000 years.
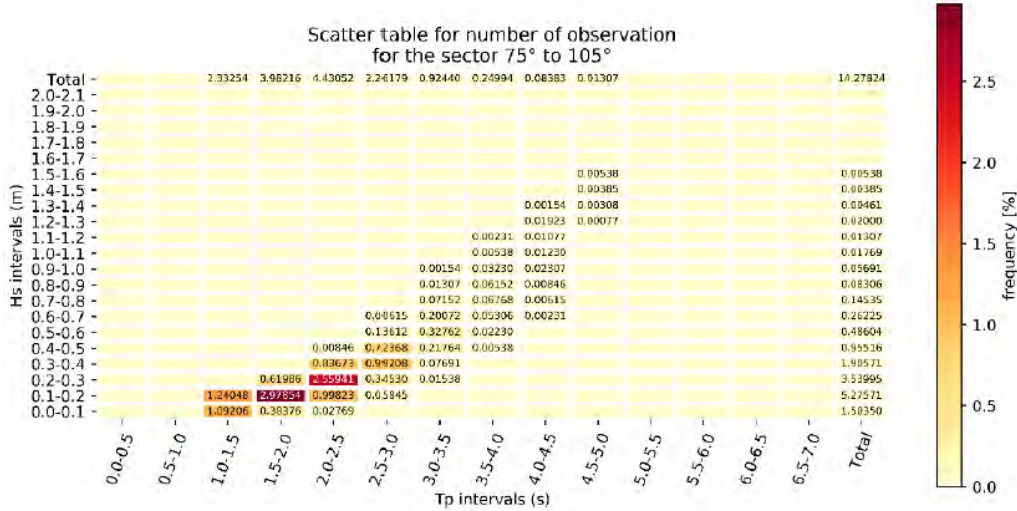

Figure 1-2 The occurrence probabilities of different sea states are given by scatter diagrams. A joint PDF $f_{H_s,T_p,\overline{\Theta}}(h,t,\theta)$ fitted to the data will be a continuous representation of the scatter diagram.

1.1.2 Short-term extreme value distribution

Within each of the $\widetilde{N}$ short-term states, the response is a stochastic process defined in terms of the parameter values (h,t,θ), illustrated by the response time-series in Figure 1-1. Since the response is a random process with different realizations for different seeds, the maximum response $\widetilde{R}$ during 1 hour will be a random variable. The cumulative distribution function (CDF) of this random variable is referred to as the short-term extreme value distribution, and we denote it by $F_{\widetilde{R}|H_s,T_p,\overline{\Theta}}(r|h,t,\theta)$ to indicate that each short-term state (h,t,θ) has its own extreme value distribution, depicted in Figure 1-3. The short-term extreme value distribution is commonly assumed to be a Gumbel distribution, which can be fitted from several response simulations for the same sea state. If the assumption of a Gaussian process is made, an analytical expression similar to the Gumbel distribution can be obtained. In this case $F_{\widetilde{R}|H_s,T_p,\overline{\Theta}}(r|h,t,\theta)$ can be established from a single frequency domain response calculation.
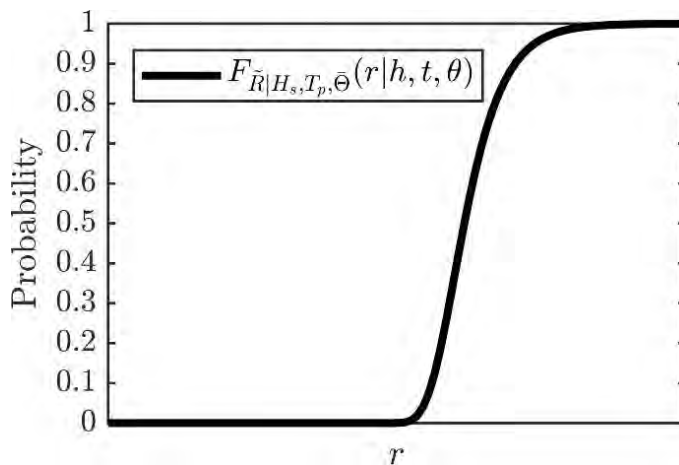

Figure 1-3 For a given sea state (h,t,θ) the short-term extreme value distribution is denoted $F_{\widetilde{R}|H_s,T_p,\overline{\Theta}}(r|h,t,\theta)$. This is determined by calculating the response for the given sea state.

1.1.3 Long-term extreme value distribution

With the long-term variation of the sea state parameters modelled by the joint PDF $f_{H_s,T_p,\overline{\Theta}}(h,t,\theta)$, and the variability in the 1-hour max described by the short-term extreme value distribution $F_{\tilde{R}|H_s,T_p,\overline{\Theta}}(r|h,t,\theta)$, the long-term distribution $F_{\tilde{R}}(r)$ of the 1-hour maximum response (the average short-term distribution) is described by the formulation

$$F_{\tilde{R}}(r) = \exp\left\{\iiint\limits_{h,t,\theta} \left(\ln F_{\tilde{R}|H_s,T_p,\overline{\Theta}}(r|h,t,\theta)\right) f_{H_s,T_p,\overline{\Theta}}(h,t,\theta)\,dh\,dt\,d\theta\right\}. \tag{2}$$

This means that the long-term distribution is obtained as an average of the short-term distributions for all sea states, weighted by the probability of occurrence of the sea states. In Eqn. (2), $F_{\tilde{R}|H_s,T_p,\overline{\Theta}}(r|h,t,\theta)$ as illustrated in Figure 1-3 represents the response calculations for each sea state, and $f_{H_s,T_p,\overline{\Theta}}(h,t,\theta)$ represents the metocean data (Figure 1-2).

The most accurate way of determining the q-probability response r_q, is to solve the integral in Eqn. (2) by numerical integration, establishing $F_{\tilde{R}}(r)$, and then identify r_q such that $1 - F_{\tilde{R}}(r_q) = q/\tilde{N}$. However, this will require a very large amount of response calculations, since the short-term extreme value distribution $F_{\tilde{R}|H_s,T_p,\overline{\Theta}}(r|h,t,\theta)$ must be established for all sea states (h,t,θ) used in the integration.

1.2 Environmental contour method (short-term design approach)

The environmental contour method offers a way to give reasonable estimates of the q-probability response r_q by performing response calculations for only a few sea states. This is sometimes referred to as the short-term design approach because r_q is estimated from the short-term distribution $F_{\tilde{R}|H_s,T_p,\overline{\Theta}}(r|h^*,t^*,\theta^*)$ of a single design sea state (h^*,t^*,θ^*), instead of establishing the long-term distribution $F_{\tilde{R}}(r)$. Estimation of the q-probability response r_q by the contour method is performed by the following points:

1. Establish environmental contours for given annual exceedance probabilities q, regarding only the environmental model $f_{H_s,T_p,\overline{\Theta}}(h,t,\theta)$ from the metocean data (Figure 1-2).

2. Identify the design sea state (h^*,t^*,θ^*) as the point along the contour than gives the most severe response.

3. Perform response calculations for the sea state (h^*,t^*,θ^*), establishing the 1-hour max distribution $F_{\tilde{R}|H_s,T_p,\overline{\Theta}}(r|h^*,t^*,\theta^*)$, and estimate the q-probability response r_q as e.g. the expected value or the 0.9-fractile of this distribution.

The first point can conveniently be executed without any regard to the structural response, considering only the metocean data, and the environmental contours are therefore reported in the metocean design basis [4]. However, it is important to be aware that there is not a unique definition of the q-probability environmental contour, and different definitions can give quite different contours, especially when contours are reported for directional sectors. Still, the environmental contours offer a simplified way of identifying sea states that are expected to give rise to the q-probability response.

The second point is typically carried out by considering a few sea states along the contour and perform response calculations for these sea states. In many cases it is the sea state with the largest value of H_s that gives the most severe response.

With the environmental contours in point 1, the randomness in the long-term response due to the environmental conditions is taken care of in a simplified manner. In point 3, if the expected 1-hour max or the median value is used to estimate the q-probability response, the randomness in the 1-hour max is not accounted for. In order to account for this, the estimate of r_q should be taken as

the p-fractile for some $p > 0.5$. An appropriate value of p should be based on experience with the relevant response type and it needs to be validated by a full long-term analysis.

The relation between the full long-term approach and the contour method is illustrated in Figure 1-4. In the full long-term approach the average short-term distribution $F_{\tilde{R}}(r)$ given by Eqn. (2) is found and the q-probability response r_q is found from an exceedance probability of $q/\tilde{N}$. When the contour method is used, a design sea state (h^*, t^*, θ^*) is found on the q-probability contour and the short-term distribution $F_{\tilde{R}|H_s,T_p,\bar{\Theta}}(r|h^*, t^*, \theta^*)$ is established for this sea state. The q-probability response r_q is then estimated by the p-fractile of this distribution.
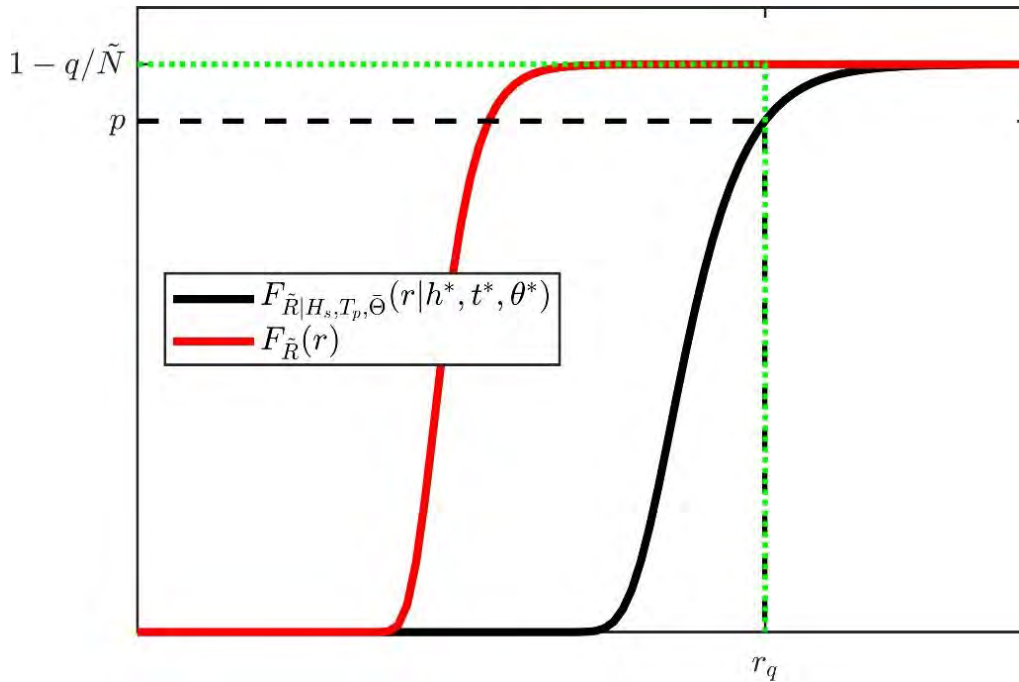

Figure 1-4 Relation between the full long-term approach and the environmental contour method.

1.3 Inverse reliability methods

In the original development of the environmental contour method [5], the environmental contours are derived from an integral similar to Eqn. (2). The variability in the short-term max response is neglected, and the integral is approximated using the first-order reliability method (FORM). Recently, methods have been developed which include variability in the 1-hour max and approximate the integral in Eqn. (2) more accurately [2, 3]. These inverse reliability methods calculate the q-probability response r_q from the full long-term formulation Eqn. (2), using approximations that make them much more efficient compared to full numerical integration. An important feature of the inverse reliability methods is that they calculate the q-probability response r_q directly through an iteration procedure. As a by-product, the iteration also produces a design point (h^*, t^*, θ^*) which should correspond to the sea state that contributes most to the long-term integral in Eqn. (2). However, this design point is not used in the same way as for the environmental contour method, since the q-probability response is already found.

2 Inverse reliability method

In this section details are presented on the applied inverse reliability method and the data that has been used as input for the method.

2.1 Environmental model

The applied environmental model has been provided by the client in terms of (H_s, T_p)-distributions for each directional sector. These are the same distributions that the environmental contours reported in the metocean design basis [4] are based on. However, the environmental contours that are reported therein have been adjusted such that the value of H_s with a given return period corresponds to the return value obtained from a peak-over-threshold (POT) analysis of the marginal H_s-distribution. Therefore, the applied environmental model is not validated for direct use in a long-term response analysis. Still, using the model can give an indication on the effect of performing a long-term response analysis.

The joint PDF $f_{H_s,T_p,\overline{\Theta}}(h, t, \theta)$ of significant wave height H_s, peak period T_p and mean wave direction $\overline{\Theta}$ is established as $f_{H_s,T_p,\overline{\Theta}}(h, t, \theta) = f_{H_s,T_p|\overline{\Theta}}(h, t|\theta)f_{\overline{\Theta}}(\theta)$. Here the mean wave direction is modelled by a piecewise constant PDF $f_{\overline{\Theta}}(\theta)$, as shown in Figure 2-1. The conditional joint PDF $f_{H_s,T_p|\overline{\Theta}}(h, t|\theta)$ is given by the (H_s, T_p)-distributions from each sector as $f_{H_s,T_p|\overline{\Theta}}(h, t|\theta) = f_{H_s,T_p}^k(h, t)$, where k refers to the sector where θ belongs.
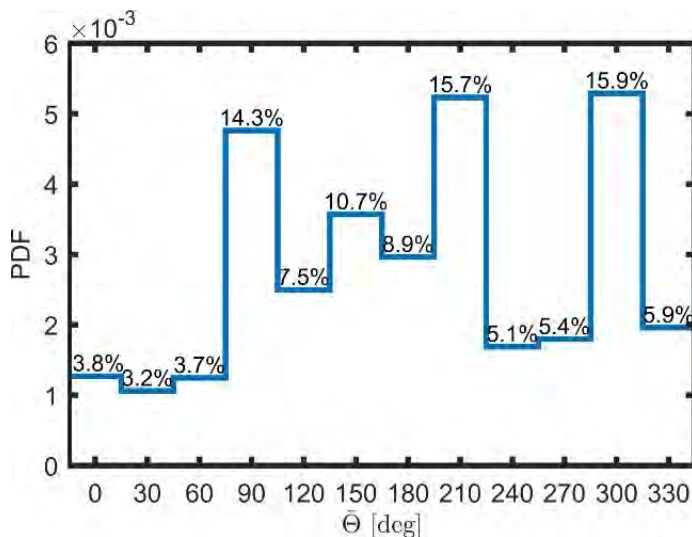

Figure 2-1 The mean wave direction is modelled by a piecewise constant PDF $f_{\overline{\Theta}}(\theta)$.

The sector probabilities are taken from the sector wise scatter tables in the metocean design basis [4]. The probability values are given in Table 2-1. The (H_s, T_p)-distributions for each sector were provided by the client, and these are given as $f_{H_s,T_p}(h, t) = f_{T_p|H_s}(t|h)f_{H_s}(h)$. The marginal distribution of H_s is given by a lognormal distribution for the lower part and a Weibull distribution for the upper part, i.e.

$$f_{H_s}(h) = \begin{cases} \dfrac{1}{\sqrt{2\pi}\sigma h} \exp\left(-\dfrac{(\ln h - \mu)^2}{2\sigma^2}\right), & \text{for } h \leq \eta, \\ \dfrac{\beta}{\rho}\left(\dfrac{h}{\rho}\right)^{\beta-1} \exp\left[-\left(\dfrac{h}{\rho}\right)^{\beta}\right], & \text{for } h > \eta. \end{cases}$$

The distribution of T_p conditional on H_s is given by a lognormal distribution with H_s-dependent parameters:

Long-term wave response

$$f_{T_p|H_s}(t|h) = \frac{1}{\sqrt{2\pi}\sigma(h)t} \exp\left(-\frac{(\ln t - \mu(h))^2}{2\sigma(h)^2}\right),$$

where $\mu(h) = a_1 + a_2 \cdot h^{a_3}$ and $\sigma(h) = b_1 + b_2 \cdot \exp(-b_3 \cdot h)$. The distribution parameters for each of the sectors is given in Table 2-2.

Table 2-1 Probability of occurence for each directional sector.

Sector	345-15	15-45	45-75	75-105	105-135	135-165
Sector probability [%]	3.8	3.2	3.7	14.3	7.5	10.7
Sector	165-195	195-225	225-255	255-285	285-315	315-345
Sector probability [%]	8.9	15.7	5.1	5.4	15.9	5.9

Table 2-2 Distribution parameters for the joint distribution of H_s and T_p within each directional sector.

Sector	μ	σ	η	ρ	β	a_1	a_2	a_3	b_1	b_2	b_3
345-15	-2,386	0,275	0,035	0,366	2,933	-7,918	9,424	0,055	0,005	0,018	0,704
15-45	-2,386	0,231	0,035	0,335	4,265	-0,504	2,225	0,399	0,005	0,018	0,032
45-75	-2,076	0,453	0,608	0,14	1,476	-2,075	3,544	0,151	0,005	0,007	2,515
75-105	-1,558	0,587	0,795	0,179	1,001	-9,028	10,406	0,041	0,005	0,007	4,266
105-135	-1,708	0,595	0,425	0,196	1,226	-3,062	4,424	0,104	0,005	0,009	3,192
135-165	-1,539	0,664	0,245	0,268	1,616	-0,591	1,88	0,284	0,005	0,008	4,303
165-195	-1,831	0,682	0,255	0,199	1,341	-21,356	22,643	0,017	0,005	0,013	0,909
195-225	-1,529	0,648	0,305	0,269	1,485	-3,861	5,229	0,088	0,005	0,004	4,344
225-255	-1,714	0,709	0,285	0,226	1,304	-1,998	3,24	0,135	0,002	0	0
255-285	-1,732	0,737	0,375	0,214	1,117	-3,927	5,18	0,078	0,002	0	0
285-315	-1,318	0,663	0,425	0,33	1,373	-65,924	67,299	0,006	0,005	0,011	4,012
315-345	-1,861	0,603	0,365	0,169	1,217	-49,822	51,28	0,008	0,005	0,019	3,09

For the environmental model $f_{H_s,T_p,\overline{\Theta}}(h,t,\theta)$ the variables $(H_s, T_p, \overline{\Theta})$ can be transformed into standard normal variables (U_1, U_2, U_3) using the Rosenblatt transformation. In the standard normal space, the contour surface that corresponds to an annual exceedance probability q will be a sphere with radius $\beta = \Phi^{-1}(1 - q/8766)$, where $\Phi(\cdot)$ is the standard normal CDF and 8766 is the number of short-term states in one year. A q-probability environmental contour surface can be obtained by transforming the sphere back to the $(H_s, T_p, \overline{\Theta})$-space using the inverse Rosenblatt transformation. This contour is thus obtained using the IFORM approach described in [5, 6]. The 100-year (0.01-probability) contour surface for the environmental model $f_{H_s,T_p,\overline{\Theta}}(h,t,\theta)$ is shown in Figure 2-2. It is seen that the contour surface is discontinuous between the sectors, since the (H_s, T_p)-distribution has different parameter values in the different sectors (cf. Table 2-2). The contour is therefore better illustrated by one plot for each sector, as given in Figure 2-3, where the directional contours given in the metocean design basis [4] are also shown. Considering Figure 2-3 it is clear that there will be a difference between using the model $f_{H_s,T_p,\overline{\Theta}}(h,t,\theta)$ and the metocean contours for estimating the long-term response. As stated above, the environmental model $f_{H_s,T_p,\overline{\Theta}}(h,t,\theta)$ is not validated for direct use in a long-term response analysis. Still, the contours shown in Figure 2-3 are not extremely different, and comparable results should still be obtained.
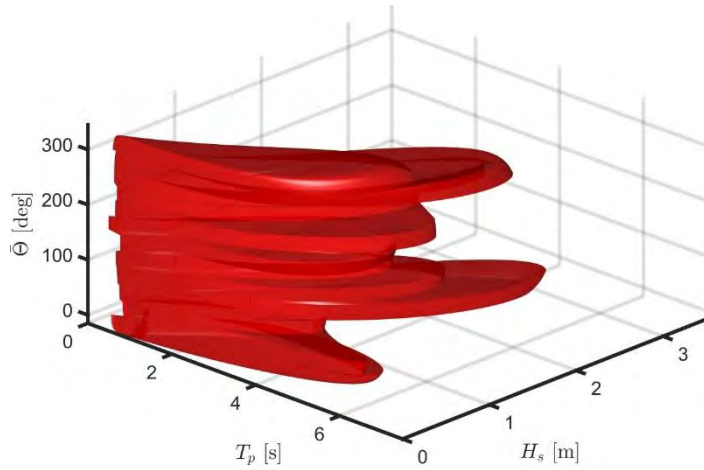
Long-term wave response

Figure 2-2 The 100-year environmental contour surface obtained from the environmental model $f_{H_s,T_p,\overline{\Theta}}(h,t,\theta)$ using the IFORM approach [6].
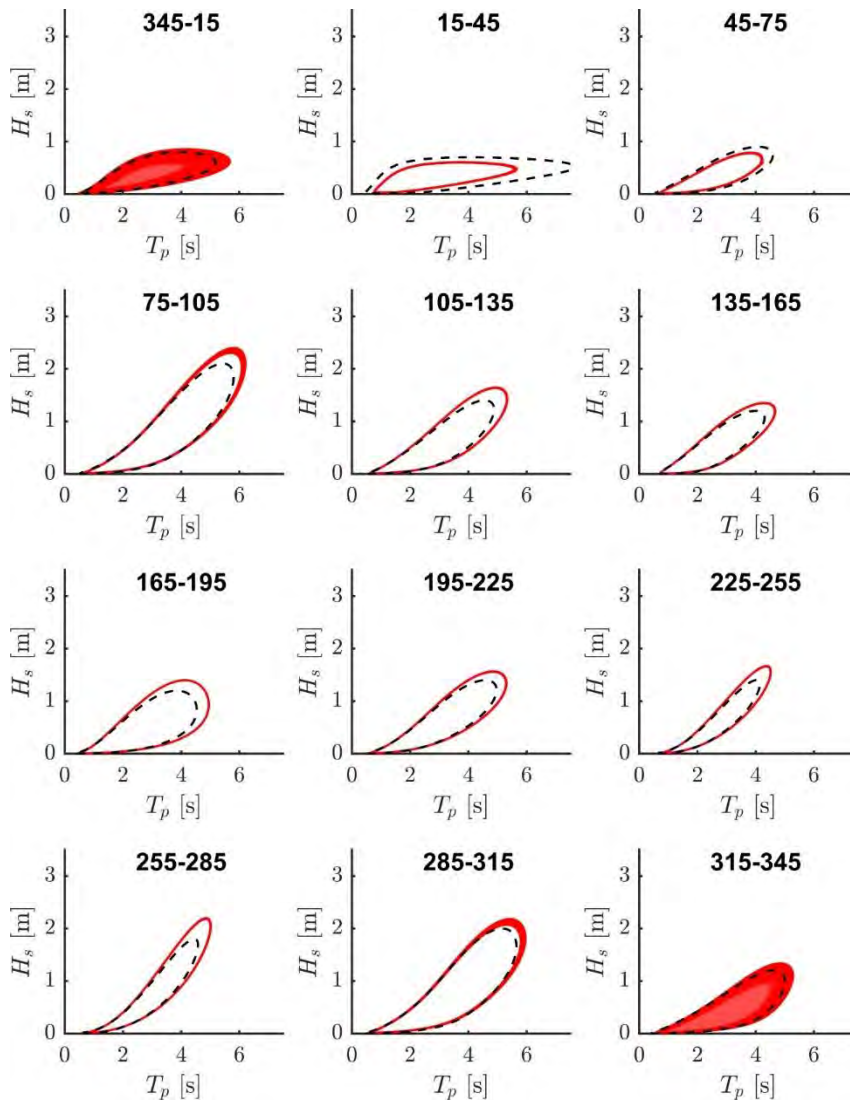

Figure 2-3 The environmental contour surface in Figure 2-2 is shown for each directional sector. The dashed lines are the directional contours given in the metocean design basis [4].

2.2 Short-term extreme value distributions

The short-term extreme value distributions $F_{\tilde{R}|H_s,T_p,\bar{\Theta}}(r|h,t,\theta)$ that have been used are obtained by assuming Gaussian response. For a Gaussian response process the short-term extreme value distribution can be expressed as

$$F_{\tilde{R}|H_s,T_p,\bar{\Theta}}(r|h,t,\theta) = \exp\left\{-\tilde{T}\sqrt{\frac{m_2(h,t,\theta)}{m_0(h,t,\theta)}}\exp\left\{-\frac{r^2}{2m_0(h,t,\theta)}\right\}\right\}, \qquad (3)$$

where $m_0(h,t,\theta)$ and $m_2(h,t,\theta)$ are the zeroth and second moments of the response spectrum $S(f)$ defined in terms of frequency (not angular frequency ω). These spectral moments are found for any sea state (h,t,θ) by performing a frequency domain response analysis for this sea state.

2.3 Choice of inverse reliability method

Different choices of inverse reliability methods exist, based on different approximations of the integral in Eqn. (2), cf. [2, 3]. First, a scaling constant C can be used to rewrite Eqn. (2), and then the choice of the inverse first- or second-order reliability method (IFORM or ISORM) is made. Herein, a scaling constant $C = 10^5$ is applied such that the method has the ability to capture design points outside the environmental contour. In order to make the implementation easier, the IFORM approach is applied. When the inverse reliability methods are applied, the q-probability response r_q and the design point (h^*,t^*,θ^*) are found by an iteration procedure. The starting point for the iteration was chosen as the sea state (h,t,θ) obtained from the simplified screening, cf. Section 3.

3   Validity of the prediction of long-term response

In the Bjørnafjorden project so far, environmental contour lines have been applied to identify which sea states that give rise to the response of a certain long-term probability of occurrence (return period). The applied methodology rests on two assumptions:

1. Along a given q-probability contour it is the sea state with the largest significant wave height that gives rise to the most severe response.
2. The q-probability response can be found by considering the 1-hour maximum for seastates along the provided q-probability contours, i.e. the contour line approach is valid.

The validity of the first assumption is checked by including more sea states on the contour line and comparing the sea states that maximizes the individual responses from this extensive screening with the simplified screening. Five sea states are selected for each contour line; maximum significant wave height, maximum peak period and three sea states in between, see Figure 3-1. Each sector is divided in smaller sub sectors with 5-degree intervals, see Figure 3-2.

The validity of the second assumption is checked by estimating the long-term response with the inverse reliability method described in Section 2. Even if the provided environmental model is not intended for a long-term response analysis, an assessment of the validity can still be made.
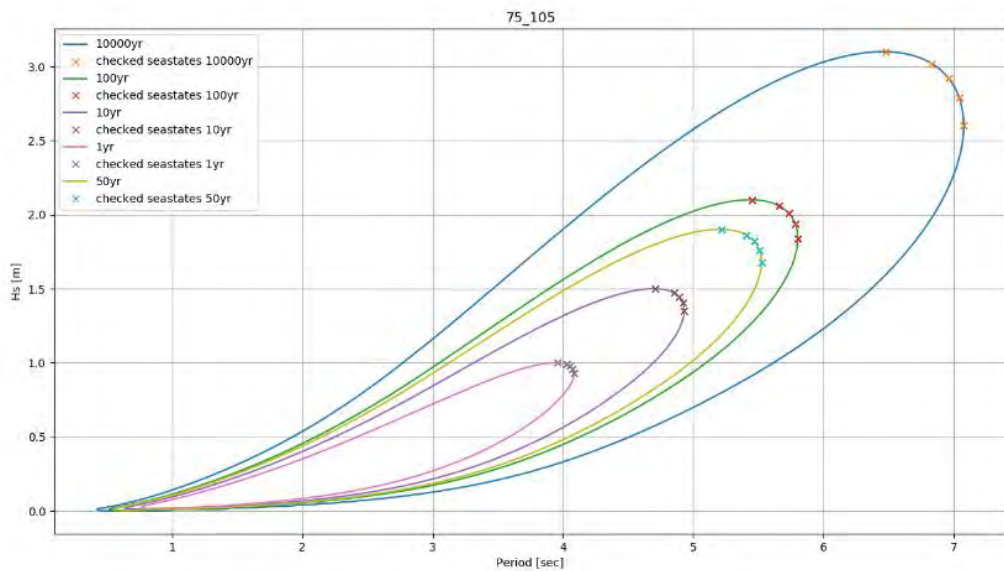

Figure 3-1 Contour lines for the sector 75-105 degrees for return periods 1, 10, 50, 100 and 10000 years. The crosses mark sea states that is run in the extensive screening.
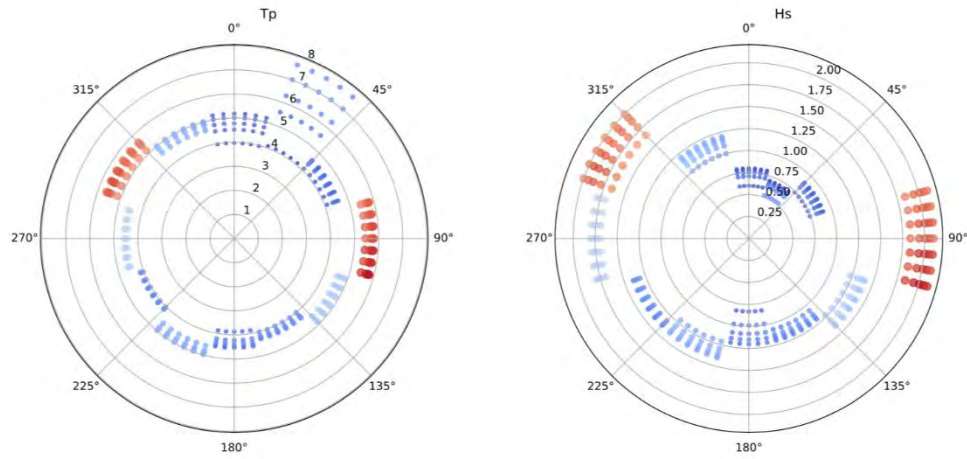
Long-term wave response

Figure 3-2: 100-year return period sea states, five sea states per direction. Each sector is divided in sub sectors with 5-degree intervals.

3.1 Validity of max Hs assumption for 100-year response

The maximum response appears for the same direction, independent on whether the sea state is selected at the maximum significant wave height or the maximum peak period or somewhere in between. This is evident from the results shown in Figure 3-3 to Figure 3-7, where the outer most points on the rose plot on the right represents the sea states at the maximum significant wave height. However, the significant wave height and peak period is shifted somewhat. In order to find the error made when estimating the response from maximum significant wave height, the response for all the five sea states are compared for the direction giving the maximum response for weak axis moments and strong axis moments in Figure 3-8 to Figure 3-12 below. The error is less than 6 % for both weak axis and strong axis moments, and the maximum response is not found at the maximum Hs but rather at a somewhat higher period. As the eigenmodes are closely spaced in this area this indicates that a slight increase in the period excites a different eigenmode in which higher response is observed for a lower wave height.

The design sea states, corresponding responses and the difference between the responses for the two different methods are summarized in Table 3-1. In Table 3-2 the selected design wave cases for the two methods are presented. Note that the global analysis used for dimensioning of the bridge components was based on the max Hs approach, but it is recommended to include also the tail of the contour line during detail design.

Table 3-1: Summary of 1 hour expected maxima for 100-year return period wind waves

		Environment						Response			
		Hs [m]		Tp [sec]		Heading [deg]		Value			
Where	**Response type/method**	max Hs	5 points	max Hs	5 points	max Hs	5 points	max Hs	5 points	Unit	diff
tower	Axial force	2.10	2.01	5.50	5.73	75	75	18.3	19.2	MN	5.4%
	Bending moment about strong axis	2.10	2.06	5.50	5.66	105	105	465.0	476.7	MNm	2.5%
	Bending moment about weak axis	1.40	2.01	4.60	5.73	200	75	0.9	0.9	MNm	4.4%
	Torsional moment	2.10	2.01	5.50	5.73	105	105	17.5	18.0	MNm	2.7%
axis 3	Axial force	2.10	2.01	5.50	5.73	75	75	17.3	18.8	MN	8.5%
	Bending moment about strong axis	2.10	2.01	5.50	5.73	105	105	393.6	406.3	MNm	3.2%
	Bending moment about weak axis	2.10	2.06	5.50	5.66	75	75	229.7	235.8	MNm	2.7%
	Torsional moment	2.10	2.10	5.50	5.45	105	105	122.4	122.0	MNm	-0.3%
axis 16	Axial force	2.10	2.01	5.50	5.73	75	75	9.9	11.0	MN	11.5%
	Bending moment about strong axis	2.10	2.01	5.50	5.73	75	75	302.8	319.7	MNm	5.6%
	Bending moment about weak axis	1.40	1.37	4.60	4.80	195	195	93.9	96.0	MNm	2.2%
	Torsional moment	2.10	2.06	5.50	5.66	105	105	58.2	58.2	MNm	0.0%
axis 38	Axial force	1.40	1.34	4.60	4.88	195	195	16.6	16.1	MN	-3.2%
	Bending moment about strong axis	2.10	2.06	5.50	5.66	75	75	416.4	427.3	MNm	2.6%
	Bending moment about weak axis	2.00	2.00	5.20	5.17	315	315	94.0	94.5	MNm	0.6%
	Torsional moment	2.10	2.01	5.50	5.73	75	75	54.4	57.0	MNm	4.8%
abutment north	Axial force	1.40	1.95	4.60	5.45	195	315	17.1	17.3	MN	1.2%
	Bending moment about strong axis	2.10	2.06	5.50	5.66	75	75	790.3	806.4	MNm	2.0%
	Bending moment about weak axis	2.00	1.95	5.20	5.45	315	315	227.3	231.0	MNm	1.6%
	Torsional moment	2.10	2.06	5.50	5.66	75	75	82.8	84.1	MNm	1.6%

Long-term wave response

Table 3-2: Selected design load cases for 100-year wind waves

	Design case 1		Design case 2		Design case 3		Design case 4	
	max hs	5 points	max hs	5 points	max hs	5 points	max hs	5 points
Hs [m]	2.1	2.01	2.1	2.06	1.4	1.34	2	2
Tp [s]	5.5	5.73	5.5	5.66	4.6	4.88	5.2	5.17
Wave Direction [deg]	75	75	105	105	195	195	315	315
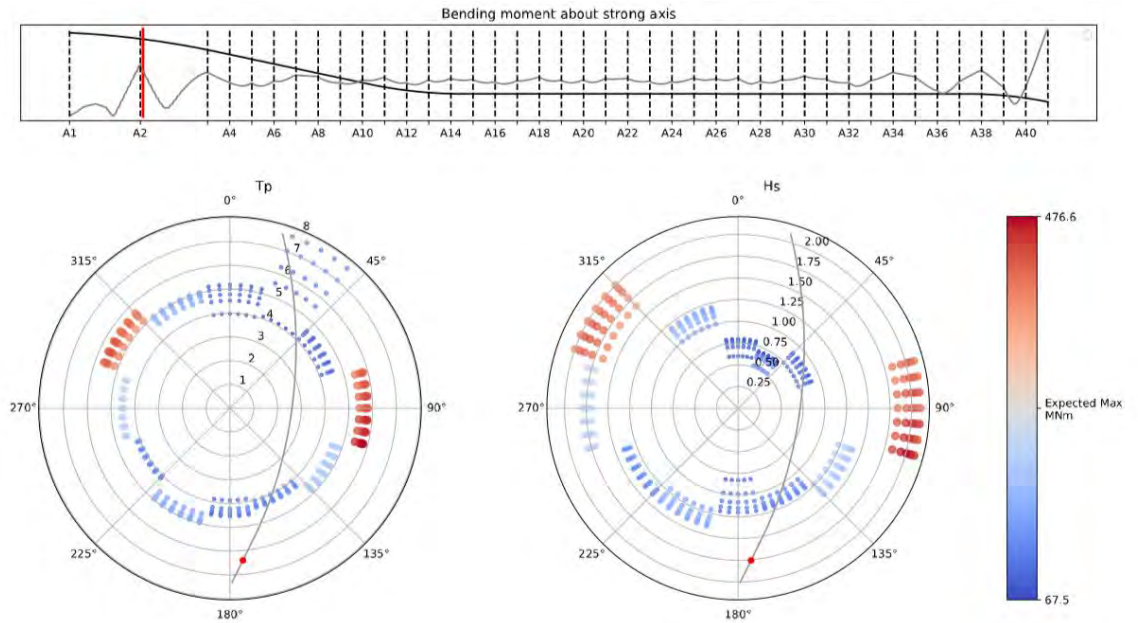
Figure 3-3: Bending moment about strong axis in the bridge girder at the tower for 100-year return period sea states along the contour.
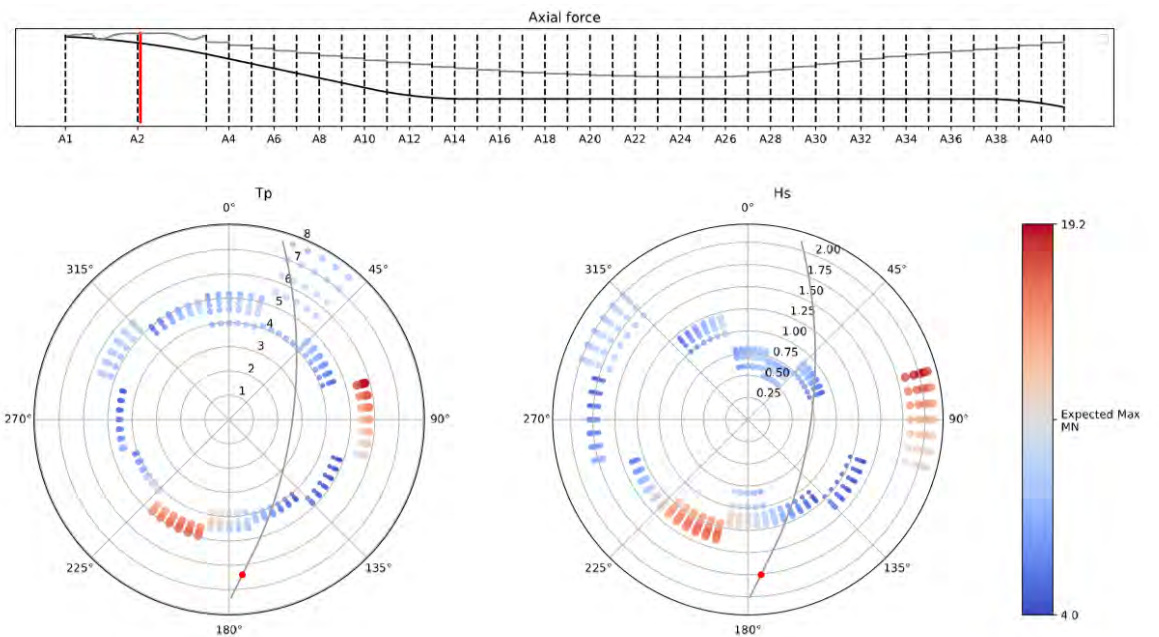
Figure 3-4: Axial force in the bridge girder at the tower for 100-year return period sea states along the contour.
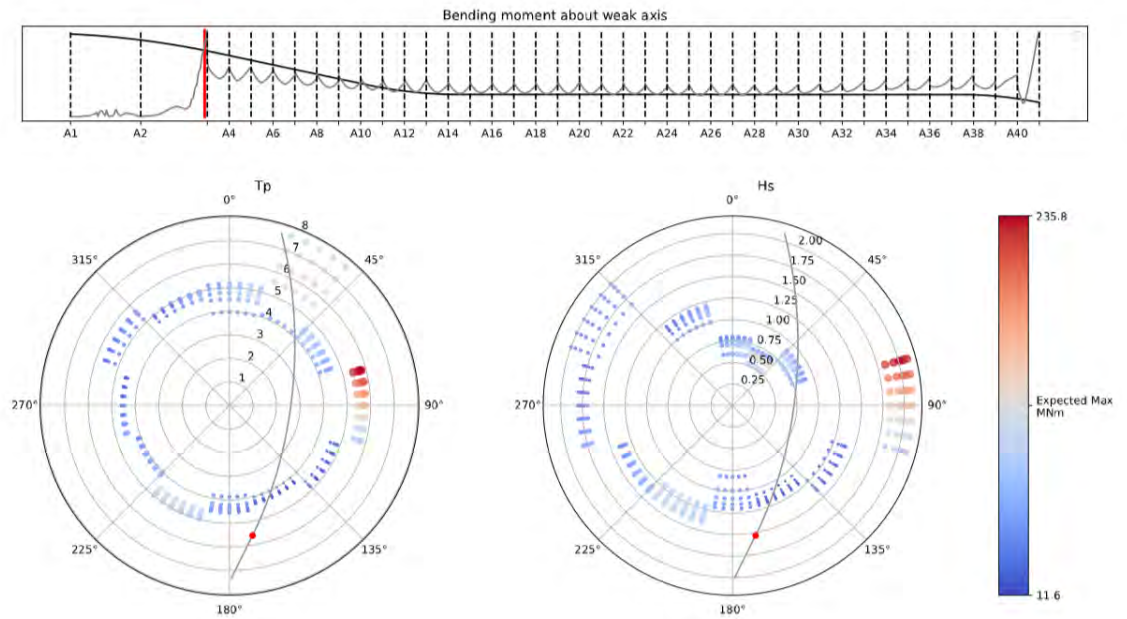
Figure 3-5: Bending moment about weak axis in the bridge girder at tower side of axis 3 for 100-year return period sea states along the contour.
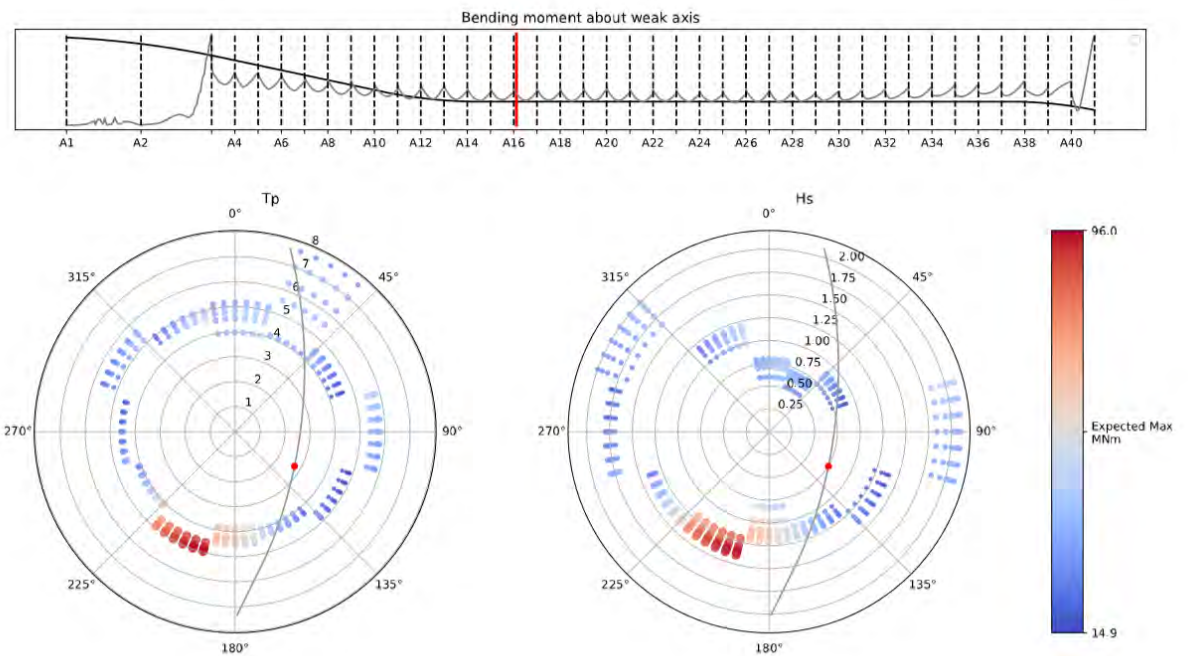
Figure 3-6: Bending moment about weak axis in the bridge girder at the north side of axis 16 for 100-year return period sea states along the contour.
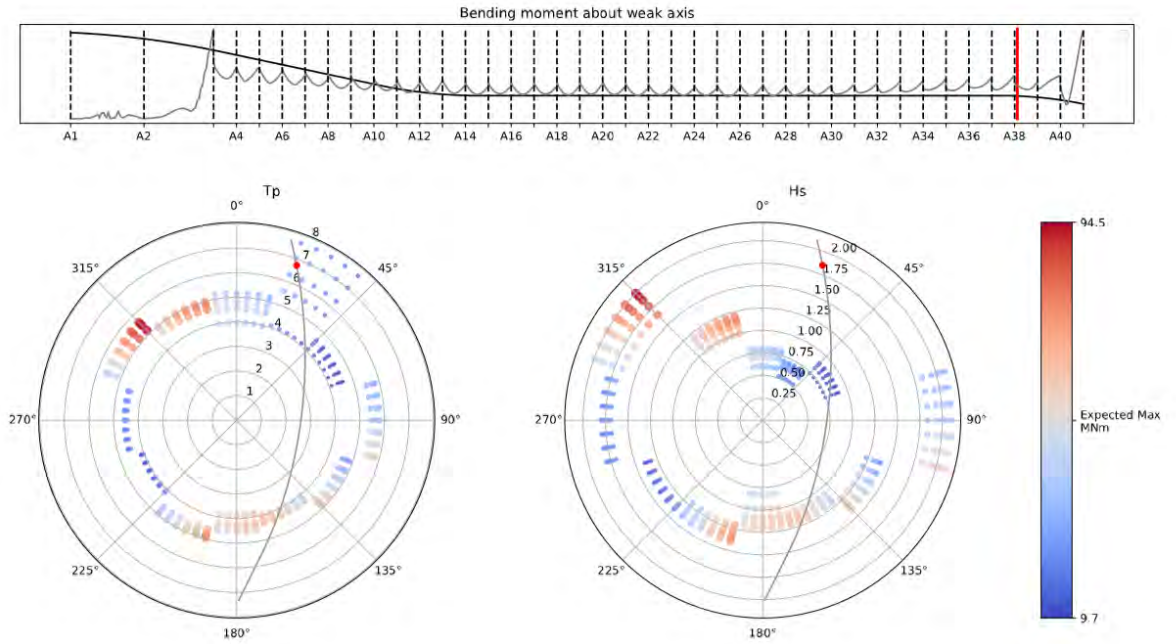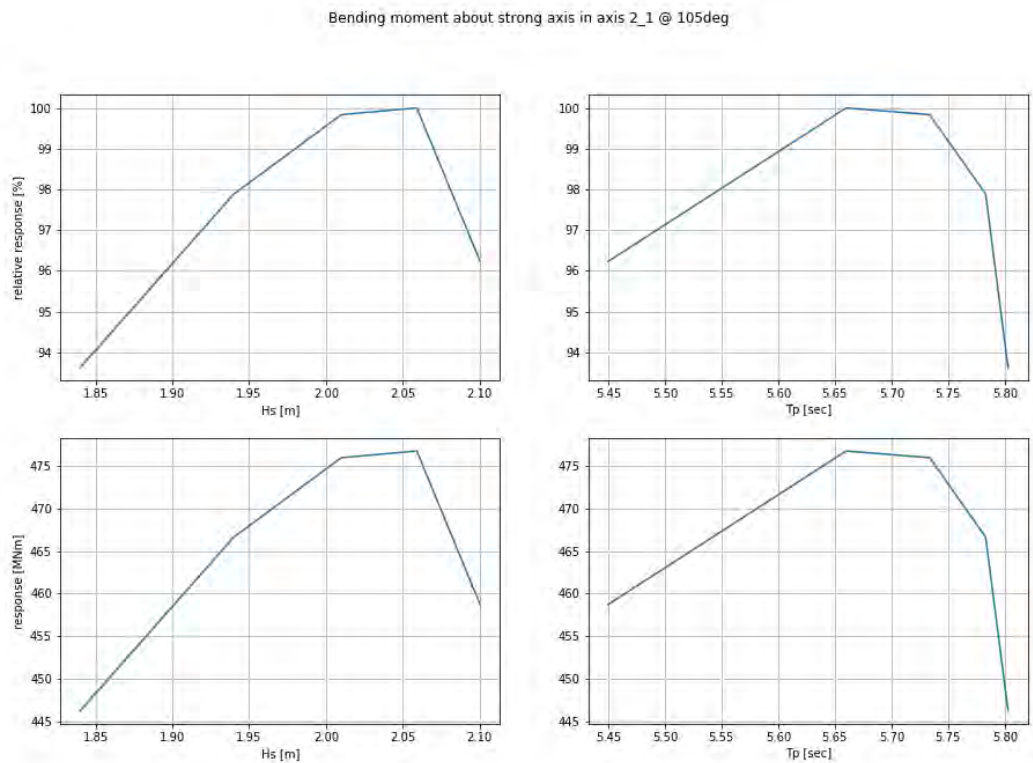
Long-term wave response

Figure 3-7: Bending moment about weak axis in the bridge girder at the north side of axis 38 for 100-year return period sea states along the contour.

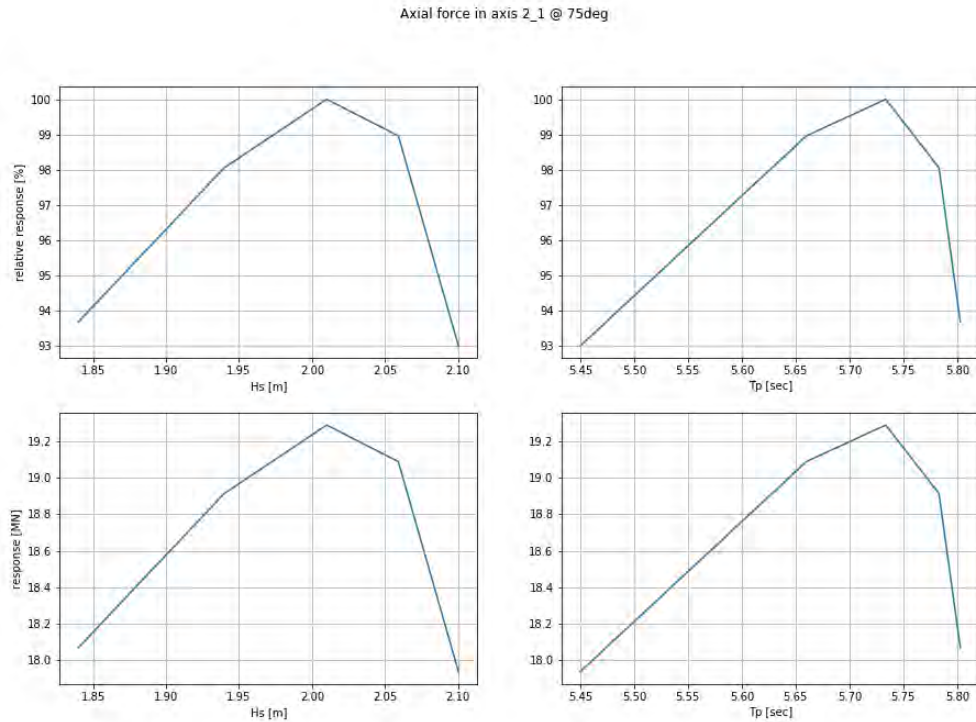*Figure 3-8: Bending moment about strong axis in the bridge girder at the tower at 105 degrees incident waves. Top plots: response relative to maximum response versus significant wave height (left) and peak period (right). Bottom plots: Actual response versus significant wave height (left) and peak period (right).*
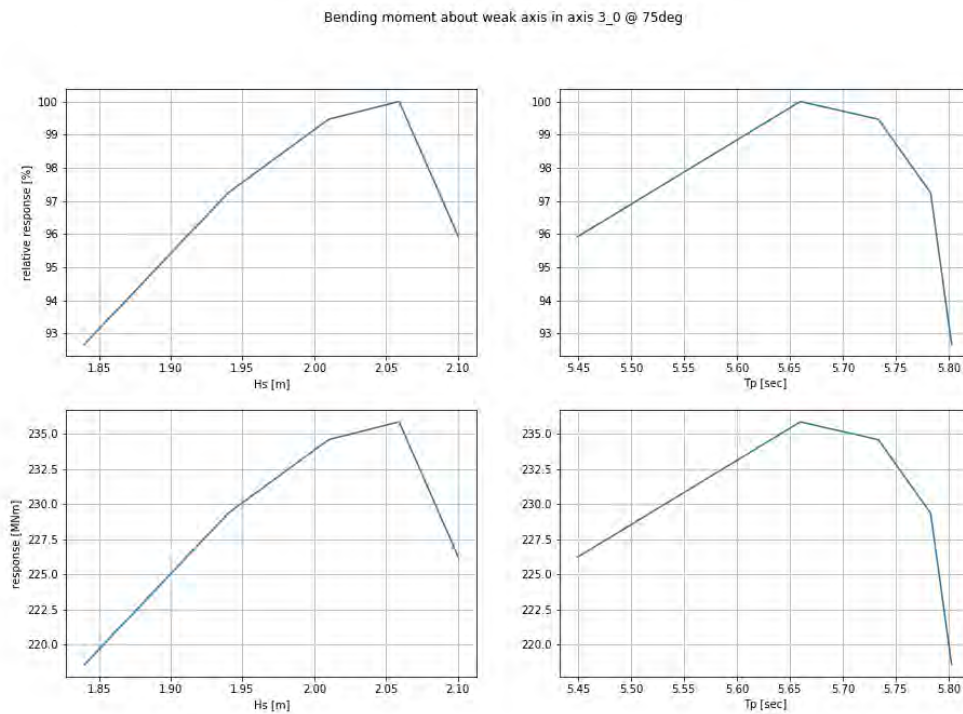
Long-term wave response

Axial force in axis 2_1 @ 75deg

Figure 3-9: Axial force in the bridge girder at the tower at 75 degrees incident waves. Top plots: response relative to maximum response versus significant wave height (left) and peak period (right). Bottom plots: Actual response versus significant wave height (left) and peak period (right).
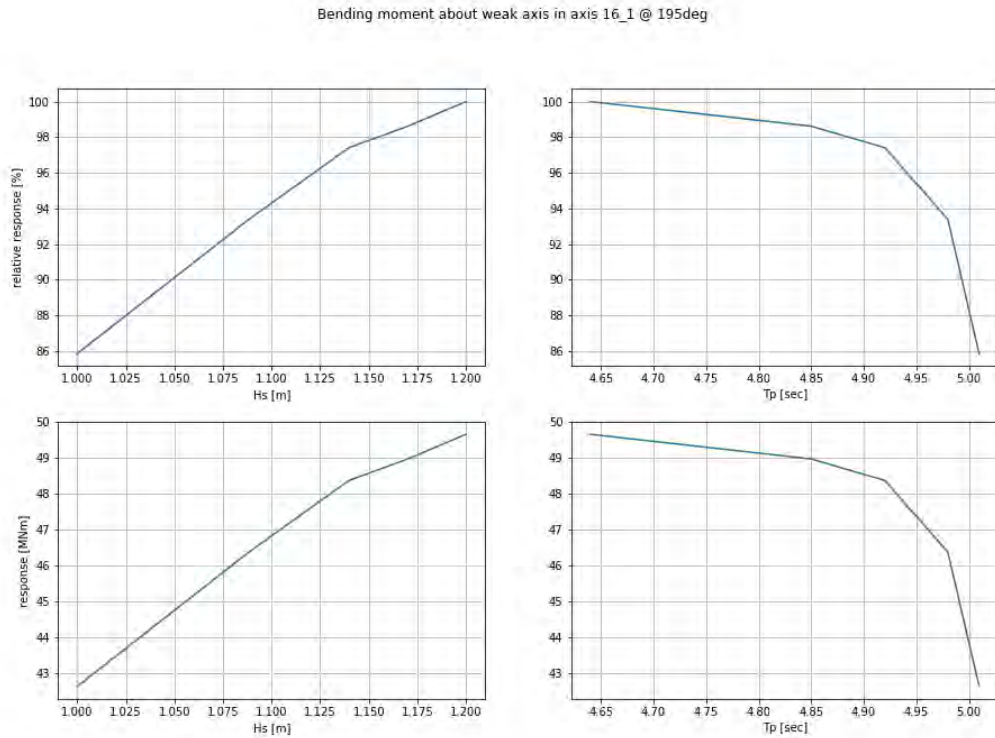
Bending moment about weak axis in axis 3_0 @ 75deg

Figure 3-10: Bending moment about weak axis in the bridge girder at the tower side of axis 3 at 75 degrees incident waves. Top plots: response relative to maximum response versus significant wave height (left) and peak period (right). Bottom plots: Actual response versus significant wave height (left) and peak period (right).

Long-term wave response

Figure 3-11: Bending moment about weak axis in the bridge girder at the tower side of axis 16 at 195 degrees incident waves. Top plots: response relative to maximum response versus significant wave height (left) and peak period (right). Bottom plots: Actual response versus significant wave height (left) and peak period (right).
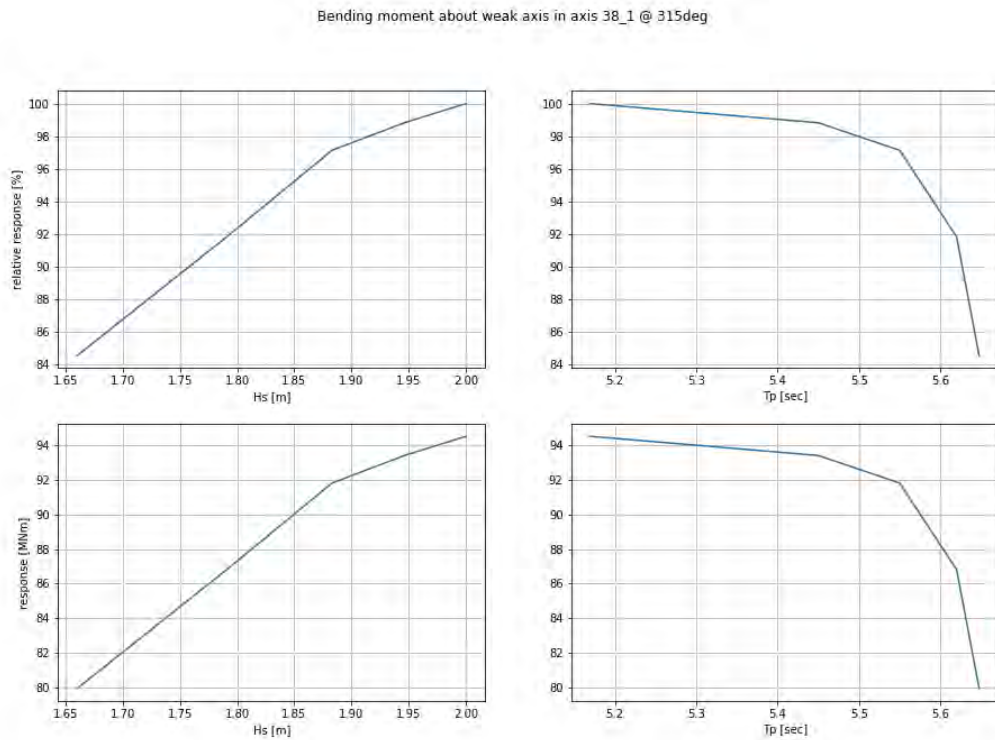

Figure 3-12: Bending moment about weak axis in the bridge girder at the north side of axis 38 at 315 degrees incident waves. Top plots: response relative to maximum response versus significant wave height (left) and peak period (right). Bottom plots: Actual response versus significant wave height (left) and peak period (right).

3.2 Validity of the contour line assumption for 100-year response

In order to assess the validity of the applied contour line approach, the 100-year response is estimated for 20 different cases using the inverse reliability method IFORM as described in Section 2. The cases are the same as those given in Table 3-1, but in all cases the response value on the south side of the axes are used, meaning that not all the results are directly comparable with Table 3-1. The results are summarized in Table 3-3, where the obtained 100-year response values are compared with the largest 1-hour expected max values obtained from the 5 points along the 100-year contour. Since the environmental model applied in the IFORM approach is not intended for direct use in long-term response prediction, too much weight should not be put into the difference in the results. Still, Table 3-3 shows that the different methods give quite similar values for the 100-year responses. A difference in 11 % is expected since the expected max and not the 90-pecentile is reported for the contour line approach. In addition, we see from Figure 2-3 that the applied environmental model gives more severe 100-year contours compared to the metocean design basis contours for the most critical sectors. Therefore, it is expected that the IFORM method will give larger response values beyond the 11 %.

Table 3-3: Comparison of 100-year wind wave response estimated by the contour line method (5 points) and the inverse reliability method (IFORM). The corresponding design points are also listed.

Where	Response type/method	Case	Hs [m]		Tp [sec]		Heading [deg]		Value		Unit	diff
			5 points	IFORM	5 points	IFORM	5 points	IFORM	5 points	IFORM		
tower	Axial force	1	2.01	2.71	5.73	6.59	75	75	19.2	31.8	MN	66 %
	Bend. mom. about strong axis	2	2.06	2.98	5.66	6.93	105	102	476.5	773.6	MNm	62 %
	Bend. mom. about weak axis	3	2.01	1.54	5.73	4.94	75	196	0.9	1.2	MNm	33 %
	Torsional moment	4	2.01	2.75	5.73	6.57	105	102	3.8	6.5	MNm	71 %
axis 3	Axial force	5	2.01	2.87	5.73	6.86	75	75	18.7	32.9	MN	76 %
	Bend. mom. about strong axis	6	2.01	2.92	5.73	6.77	105	102	406.3	664.3	MNm	63 %
	Bend. mom. about weak axis	7	2.06	2.75	5.66	6.45	75	75	235.8	337.2	MNm	43 %
	Torsional mom.	8	2.10	2.92	5.45	6.58	105	105	72.1	149.7	MNm	108 %
axis 16	Axial force	9	2.01	2.98	5.73	6.94	75	94	11.3	23.1	MN	104 %
	Bend. mom. about strong axis	10	2.01	2.89	5.73	6.95	75	75	320.6	509.1	MNm	59 %
	Bend. mom. about weak axis	11	1.37	1.59	4.80	5.07	195	195	84.5	106.8	MNm	26 %
	Torsional moment	12	2.06	2.81	5.66	6.55	105	105	59.9	90.8	MNm	52 %
axis 38	Axial force	13	1.34	1.40	4.88	4.60	195	195	15.8	20.2	MN	28 %
	Bend. mom. about strong axis	14	2.06	2.92	5.66	6.87	75	85	426.7	702.4	MNm	65 %
	Bend. mom. about weak axis	15	2.00	2.26	5.17	5.71	315	315	113.4	137.1	MNm	21 %
	Torsional moment	16	2.01	2.78	5.73	6.45	75	75	53.4	75.9	MNm	42 %
abutment north	Axial force	17	1.95	2.84	5.45	6.94	315	105	17.3	28.5	MN	65 %
	Bend. mom. about strong axis	18	2.06	2.25	5.66	5.70	75	78	806.3	1018.9	MNm	26 %
	Bend. mom. about weak axis	19	1.95	2.34	5.45	5.84	315	315	230.9	265	MNm	15 %
	Torsional moment	20	2.06	2.72	5.66	6.35	75	75	84	116.1	MNm	38 %

The assumption that the 100-year response is most likely to occur for a sea state along the environmental contour can be checked by comparing the design point obtained from the IFORM method with the contours. In Figure 3-13 to Figure 3-32, the design points obtained from the IFORM method are shown along with the environmental contours for the cases summarized in Table 3-3. For the cases displayed in Figure 3-15, Figure 3-23, Figure 3-25, Figure 3-27, Figure 3-30 and Figure 3-31 we see that the design point is quite close to the 100-year contours of the applied environmental model. These cases correspond respectively to cases number 3, 11, 13, 15, 18 and 19 in Table 3-3, and these are the ones where the difference between the 5 point screening and the IFORM method is the smallest (roughly 20-30 %). If 11 % of the difference in response is explained by using the 90-percentile, this indicates that an additional increase of roughly 10-20 % is due to the difference in the contours.

For the other cases, however, the design point is seen to be located further outside the contours, giving a difference in the estimated 100-year response of roughly 60 % for most of the cases and 108 % for the worst case. An explanation for this increased difference could be that the environmental contours are derived based on an approximation that is unconservative in these cases. The environmental contour (red surface) in Figure 2-2 and Figure 2-3 is based on a FORM approximation of the long-term integral [5], and this is not necessarily conservative. The applied IFORM method is also based on a FORM approximation, but for this method the long-term integral is modified using a scaling constant $C = 10^5$ which has been shown to improve the approximation [2]. Still, there is an uncertainty in the results obtained by this method also. In order to obtain the actual 100-year response, the long-term integral must be solved using numerical integration.

It should be noted that since the IFORM method estimates the 100-year response directly, the design point obtained from the IFORM method is not meant to be used in the same way as a design point along the contour. Still, the IFORM design point is an approximation to the sea state that contributes most to the 100-year response [2, 3]. If this sea state does not correspond well with the environmental contour, it could be an indication that the contour method underestimates the 100-year response.

The uncertainties in the contour line approach can be summarized as follows:

1. Uncertainty due to variability in the short-term response. This is can be accounted for in a simplified manner by using the p-fractile of the 1-hour extreme distribution. An appropriate value of p should be based on experience. If the 90-percentile is used instead of the expected max for a Gaussian process, this correction corresponds to an increase of 11 % in the 100-year response.

2. Uncertainty in the environmental contours. Environmental contours corresponding to a given return period are not uniquely defined. Different methods exist to produce them, and these can give quite different results [7, 8, 9], especially when sector dependence is included [10].

Even if the results in this section are based on an environmental model that is not validated for use in long-term response estimation, they give an indication that the estimates of the long-term response produced by the contour line approach might be too rough in some cases. However, it is not possible to draw any definite conclusion without a comparison with a full long-term approach. Further studies on the long-term response are therefore recommended. An environmental model suited for use in long-term response analyses should be established, and full integration of the long-term response formulation should be carried out for some selected cases.
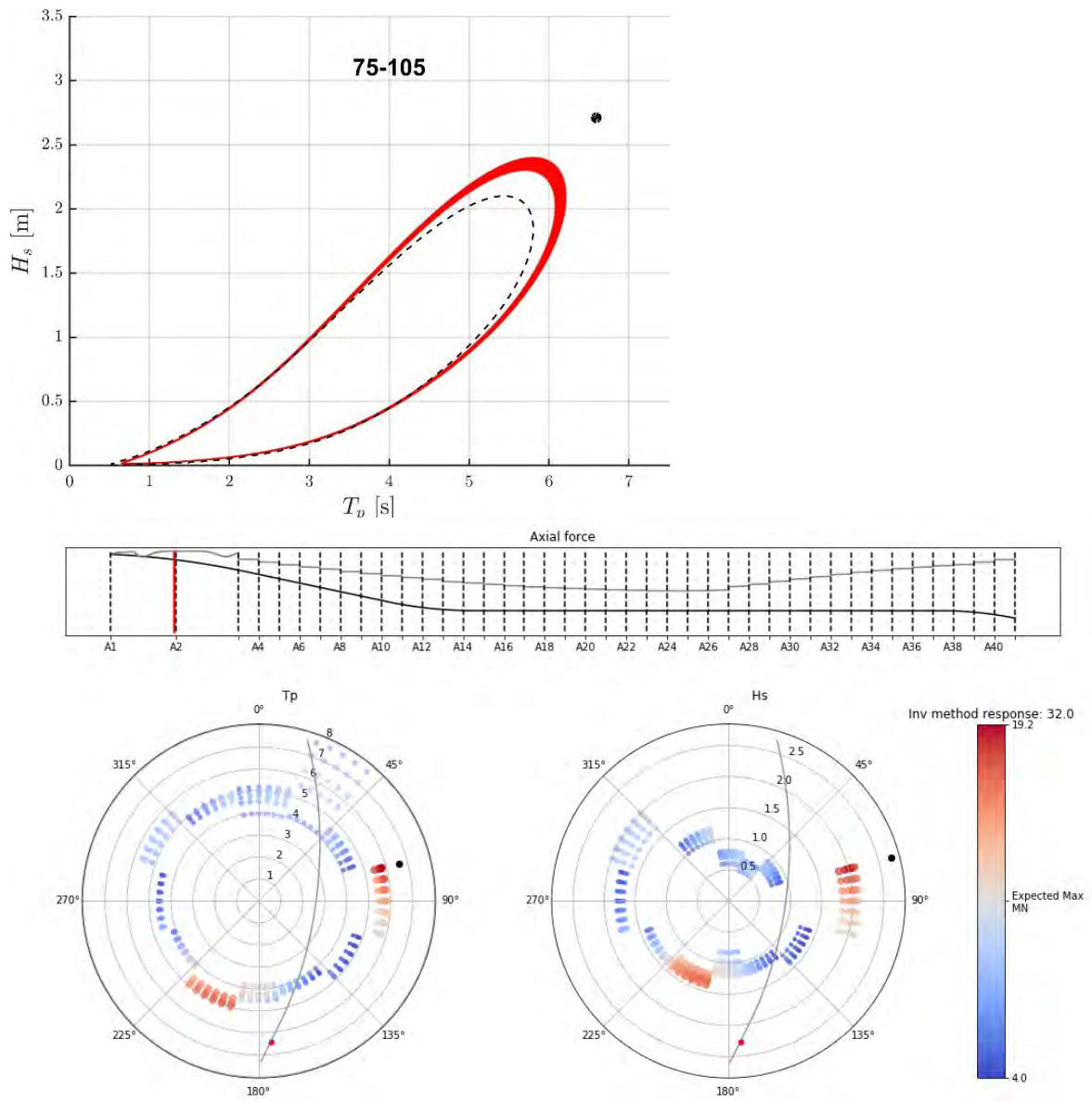
Long-term wave response

Figure 3-13: Case 1. Axial force in the bridge girder at the south side of axis 2 (the tower) for 100-year return period sea states along the contour, plotted together with the IFORM design point (black dot). The IFORM response is indicated above the colour bar. The top figure shows the IFORM design point along with the environmental contours for the relevant sector, cf. Figure 2-3.
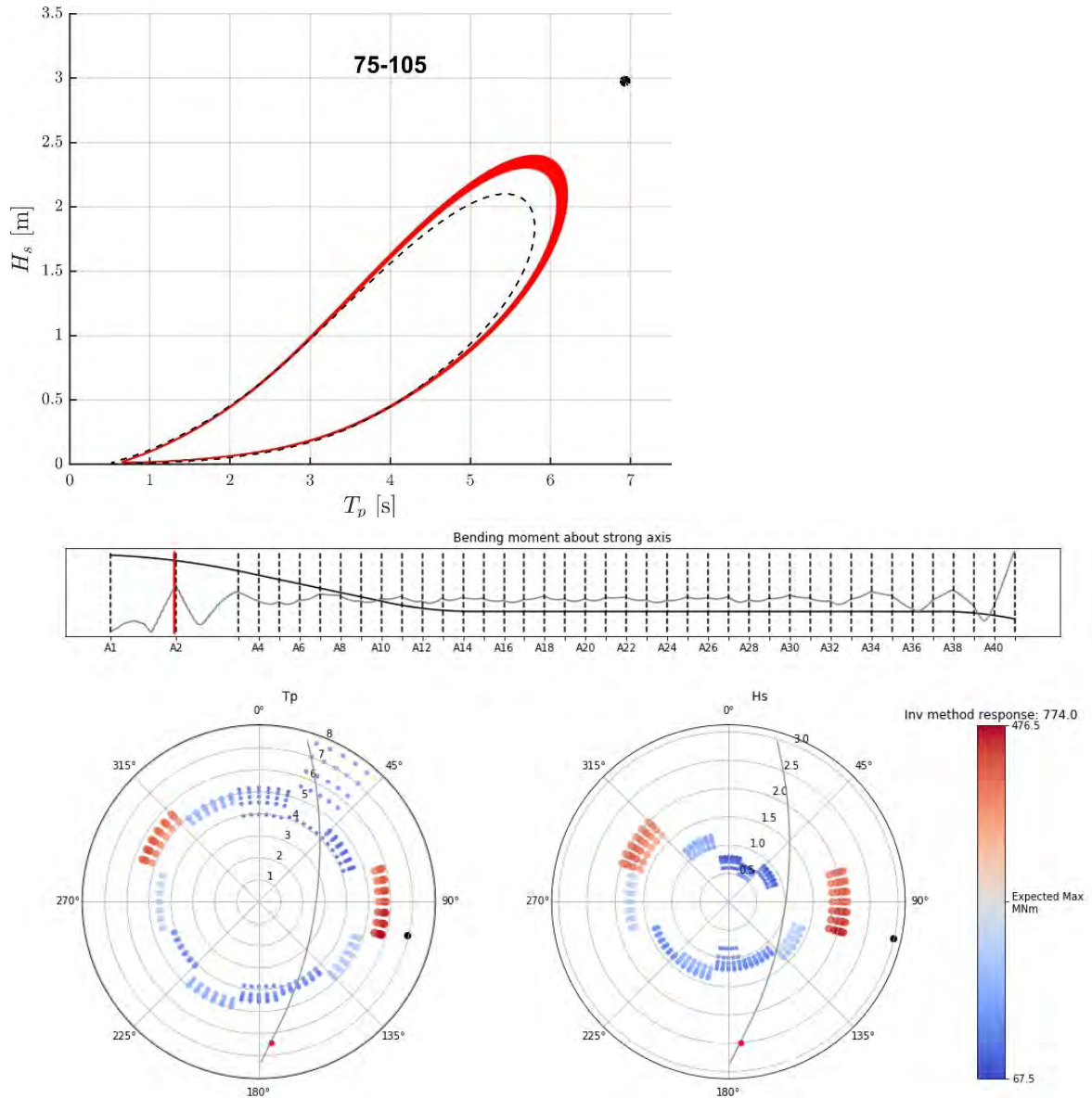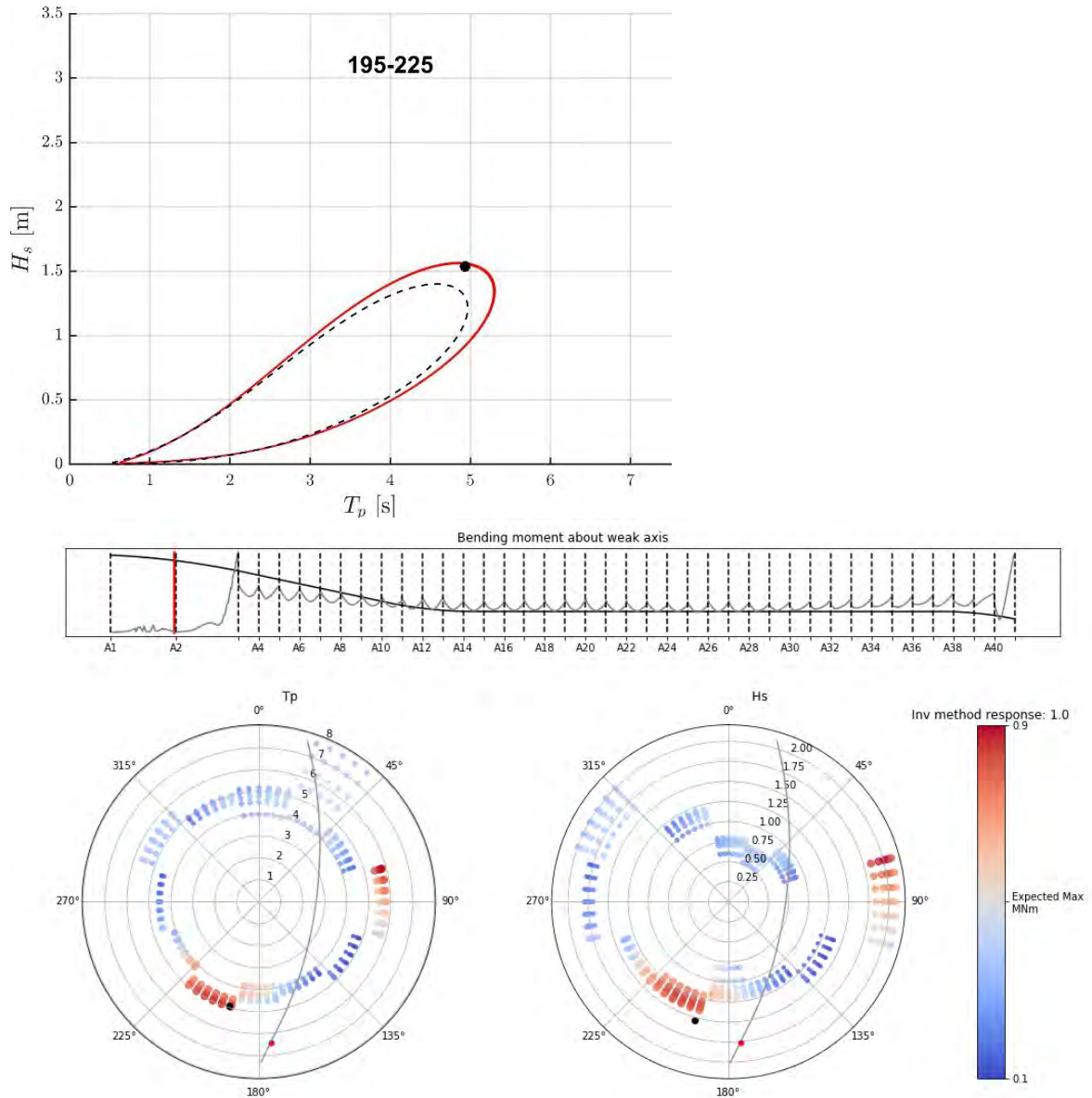
Long-term wave response

Figure 3-14: Case 2. Bending moment about strong axis in the bridge girder at the south side of axis 2 (the tower) for 100-year return period sea states along the contour, plotted together with the IFORM design point (black dot). The IFORM response is indicated above the colour bar. The top figure shows the IFORM design point along with the environmental contours for the relevant sector, cf. Figure 2-3.
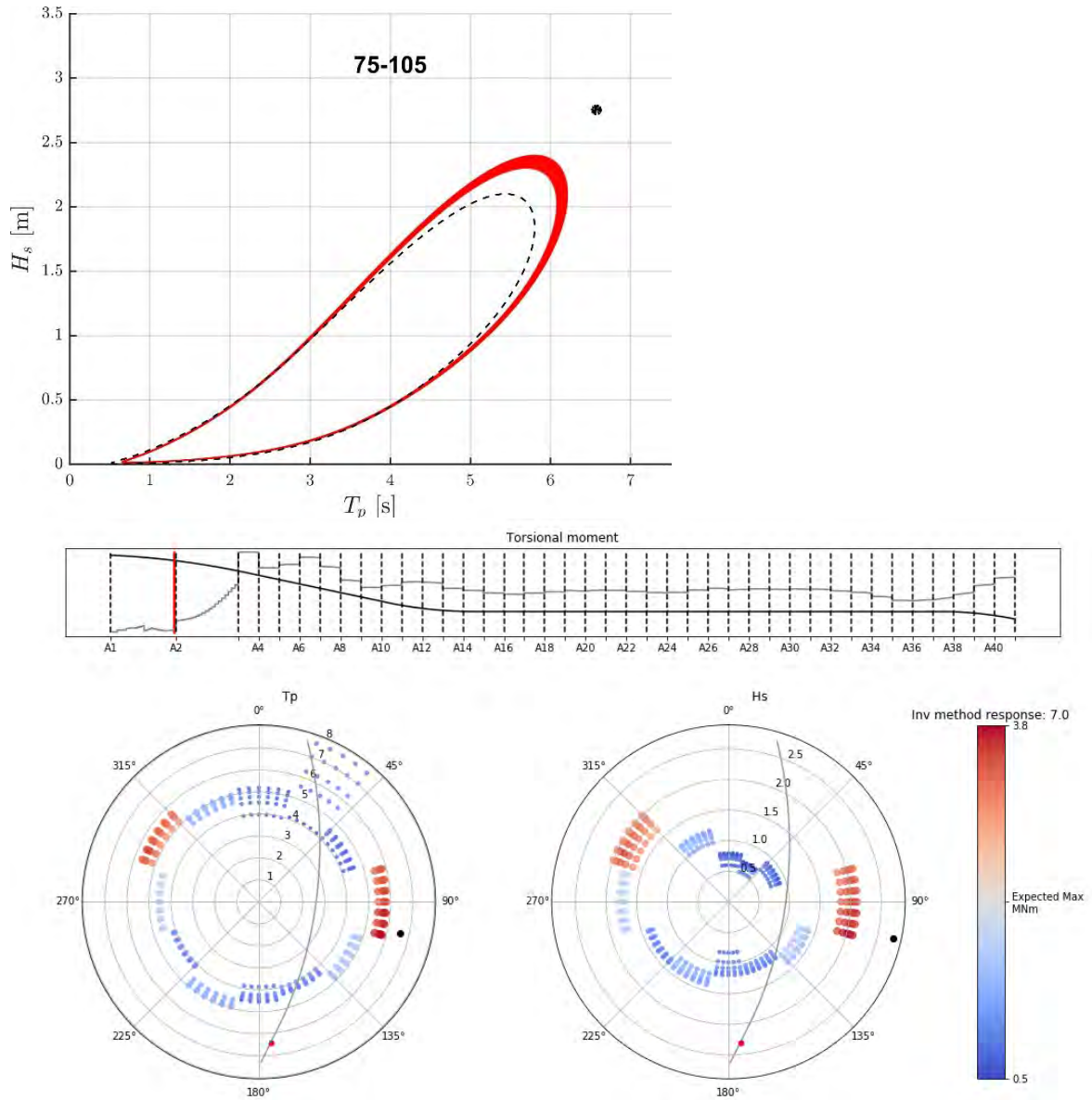
Long-term wave response

Figure 3-15: Case 3. Bending moment about weak axis in the bridge girder at the south side of axis 2 (the tower) for 100-year return period sea states along the contour, plotted together with the IFORM design point (black dot). The IFORM response is indicated above the colour bar. The top figure shows the IFORM design point along with the environmental contours for the relevant sector, cf. Figure 2-3.
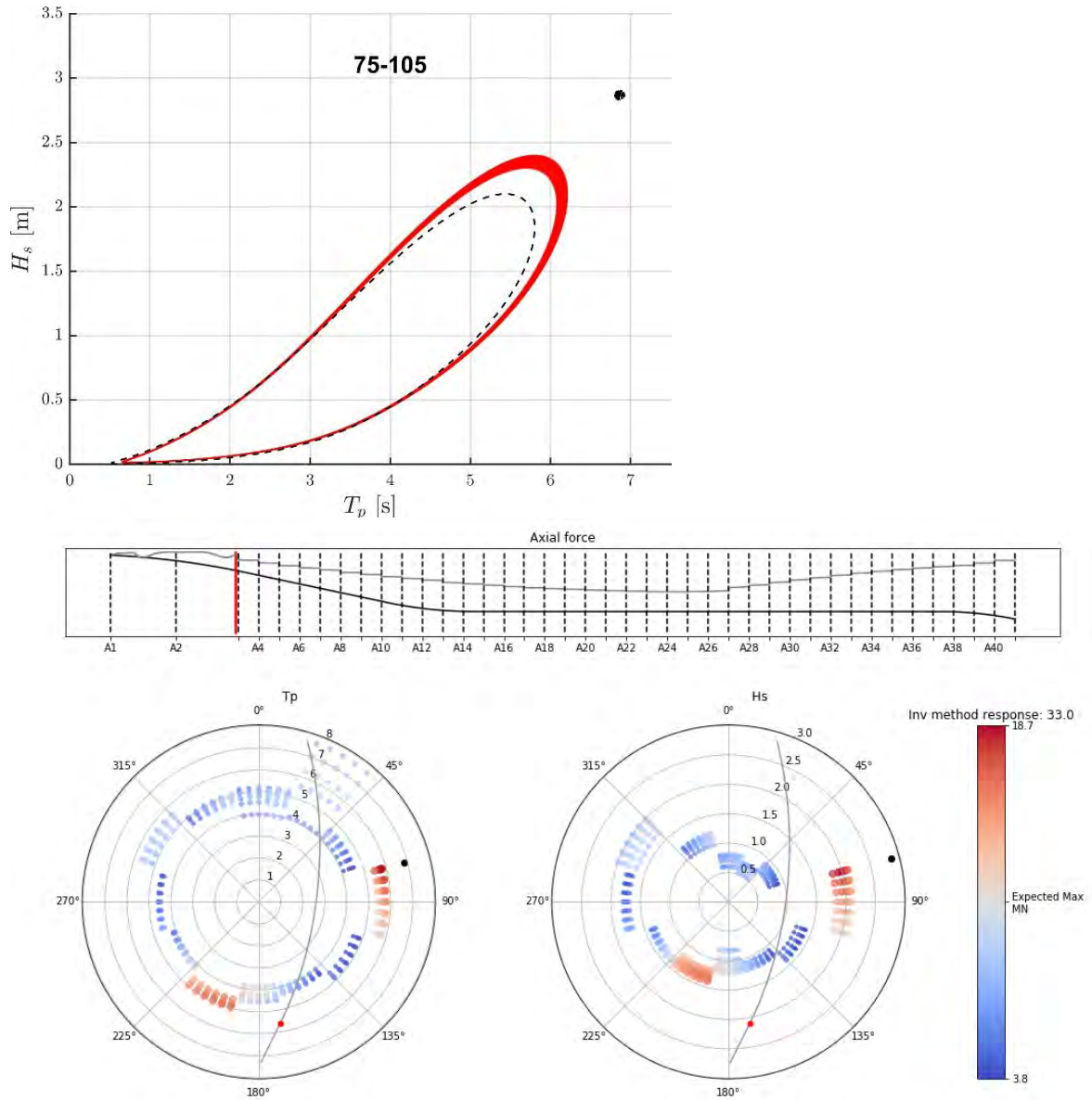
Long-term wave response

Figure 3-16: Case 4. Torsional moment in the bridge girder at the south side of axis 2 (the tower) for 100-year return period sea states along the contour, plotted together with the IFORM design point (black dot). The IFORM response is indicated above the colour bar. The top figure shows the IFORM design point along with the environmental contours for the relevant sector, cf. Figure 2-3.
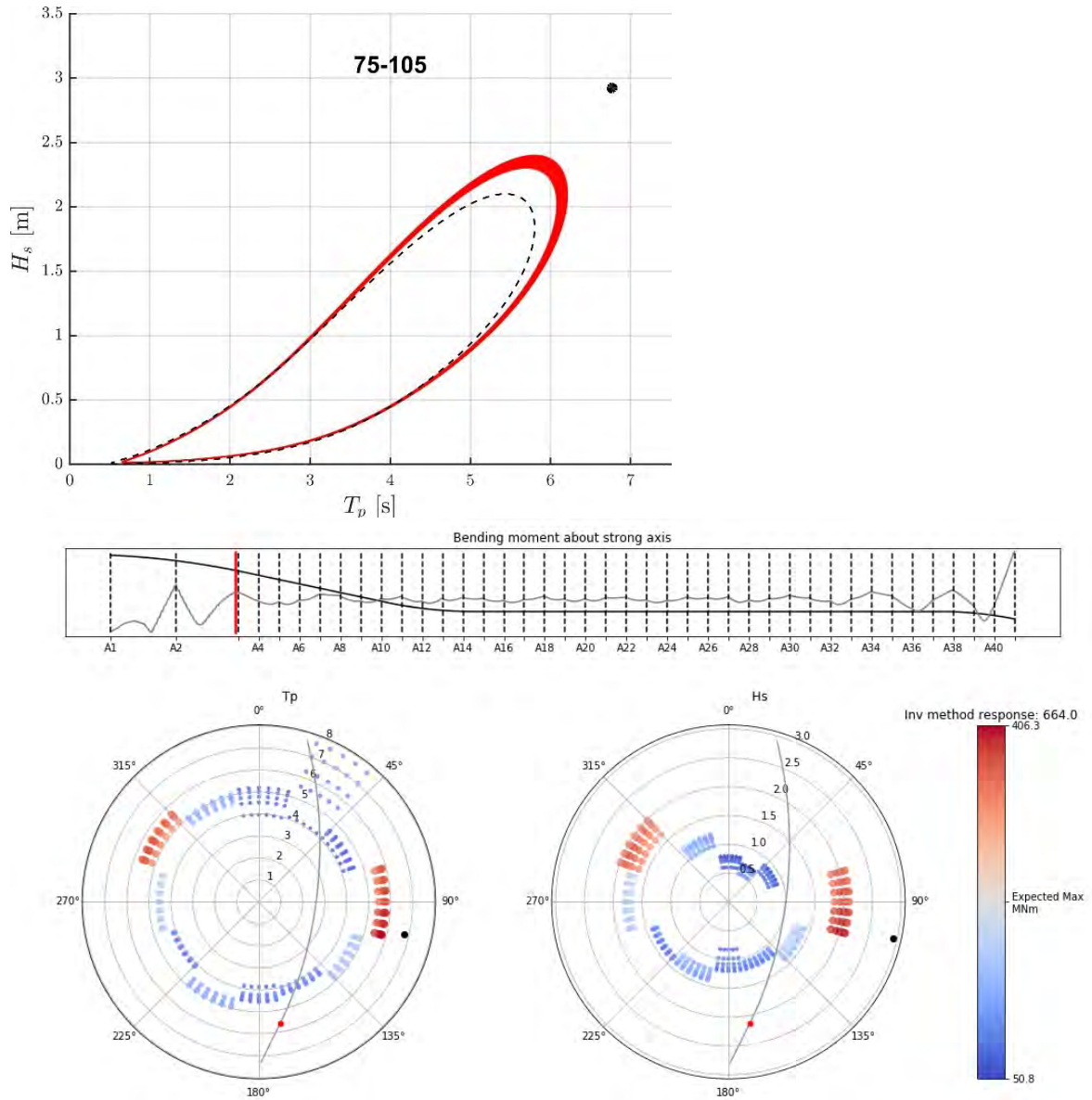
Long-term wave response

Figure 3-17: Case 5. Axial force in the bridge girder at the south side of axis 3 for 100-year return period sea states along the contour, plotted together with the IFORM design point (black dot). The IFORM response is indicated above the colour bar. The top figure shows the IFORM design point along with the environmental contours for the relevant sector, cf. Figure 2-3.

Long-term wave response

Figure 3-18: Case 6. Bending moment about strong axis in the bridge girder at the south side of axis 3 for 100-year return period sea states along the contour, plotted together with the IFORM design point (black dot). The IFORM response is indicated above the colour bar. The top figure shows the IFORM design point along with the environmental contours for the relevant sector, cf. Figure 2-3.
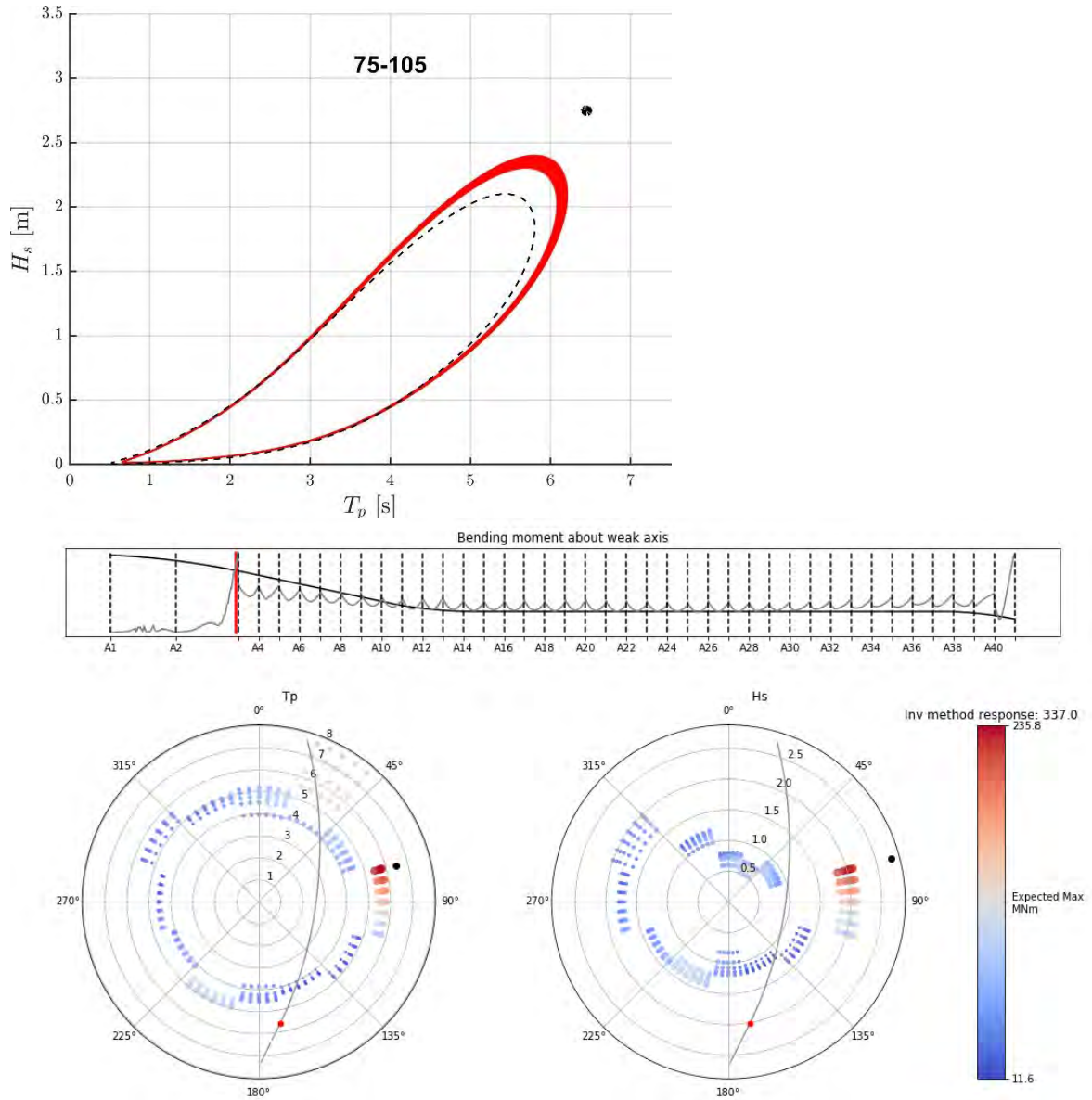
Long-term wave response

Figure 3-19: Case 7. Bending moment about weak axis in the bridge girder at the south side of axis 3 for 100-year return period sea states along the contour, plotted together with the IFORM design point (black dot). The IFORM response is indicated above the colour bar. The top figure shows the IFORM design point along with the environmental contours for the relevant sector, cf. Figure 2-3.
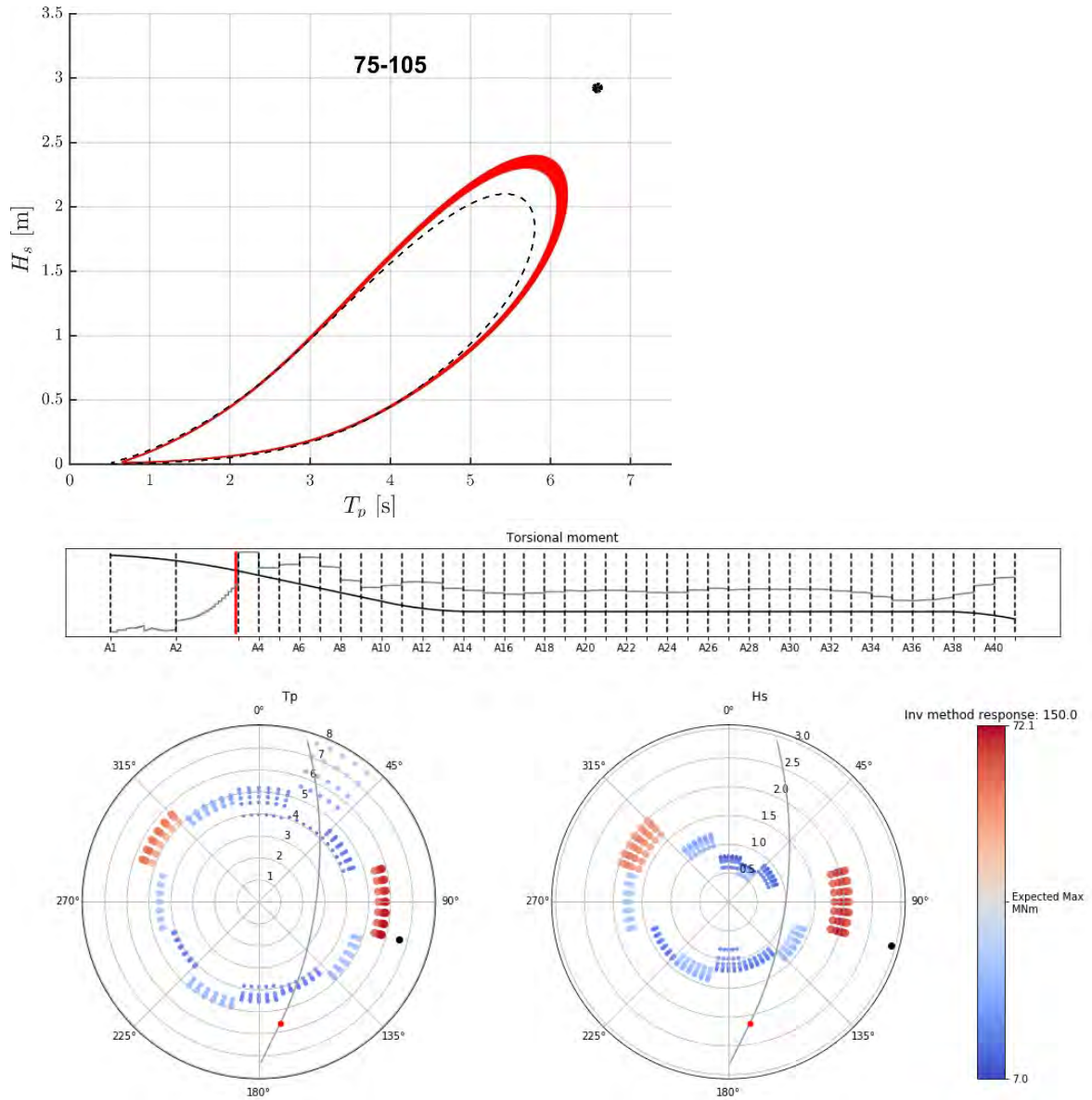
Long-term wave response

Figure 3-20: Case 8. Torsional moment in the bridge girder at the south side of axis 3 for 100-year return period sea states along the contour, plotted together with the IFORM design point (black dot). The IFORM response is indicated above the colour bar. The top figure shows the IFORM design point along with the environmental contours for the relevant sector, cf. Figure 2-3.